



**HAL**  
open science

## Dynamical tide in stellar radiative zones

J. Ahuir, S. Mathis, L. Amard

► **To cite this version:**

J. Ahuir, S. Mathis, L. Amard. Dynamical tide in stellar radiative zones: General formalism and evolution for low-mass stars. *Astronomy and Astrophysics - A&A*, 2021, 651, pp.A3. 10.1051/0004-6361/202040174 . hal-03296053

**HAL Id: hal-03296053**

**<https://hal.science/hal-03296053>**

Submitted on 22 Jul 2021

**HAL** is a multi-disciplinary open access archive for the deposit and dissemination of scientific research documents, whether they are published or not. The documents may come from teaching and research institutions in France or abroad, or from public or private research centers.

L'archive ouverte pluridisciplinaire **HAL**, est destinée au dépôt et à la diffusion de documents scientifiques de niveau recherche, publiés ou non, émanant des établissements d'enseignement et de recherche français ou étrangers, des laboratoires publics ou privés.

# Dynamical tide in stellar radiative zones

## General formalism and evolution for low-mass stars

J. Ahuir<sup>1</sup>, S. Mathis<sup>1</sup>, and L. Amard<sup>2</sup>

<sup>1</sup> Département d’Astrophysique-AIM, CEA/DRF/IRFU, CNRS/INSU, Université Paris-Saclay, Université Paris-Diderot, Université de Paris, 91191 Gif-sur-Yvette, France  
e-mail: jeremy.ahuir@cea.fr

<sup>2</sup> Department of Physics & Astronomy, University of Exeter, Stoker Road, Devon Exeter EX4 4QL, UK

Received 18 December 2020 / Accepted 11 April 2021

### ABSTRACT

**Context.** Most exoplanets detected so far are close-in planets, which are likely to be affected by tidal dissipation in their host star. To obtain a complete picture of the evolution of star–planet systems, we need to consider the effect of tides within stellar radiative and convective zones.

**Aims.** We aim to provide a general formalism allowing us to assess tidal dissipation in stellar radiative zones for late- and early-type stars, including stellar structure with a convective core and an envelope like in F-type stars. This allows us to study the dynamics of a given system throughout the stellar evolution. On this basis, we investigate the effect of stellar structure and evolution on tidal dissipation in the radiative core of low-mass stars.

**Methods.** We developed a general theoretical formalism to evaluate tidal dissipation in stellar radiative zones that is applicable to early- and late-type stars. From the study of adiabatic oscillations throughout the star, we computed the energy flux transported by progressive internal gravity waves and the induced tidal torque. By relying on grids of stellar models, we studied the effect of stellar structure and evolution on the tidal dissipation of F-, G-, and K-type stars from the pre-main sequence (PMS) to the red giant branch (RGB).

**Results.** For a given star–planet system, tidal dissipation reaches a maximum value on the PMS for all stellar masses. On the main sequence (MS), it decreases to become almost constant. The dissipation is then several orders of magnitude smaller for F-type than for G- and K-type stars. During the subgiant phase and the RGB, tidal dissipation increases by several orders of magnitude, along with the expansion of the stellar envelope. We show that the dissipation of the dynamical tide in the convective zone dominates the evolution of the system during most of the PMS and the beginning of the MS, as the star rotates rapidly. Tidal dissipation in the radiative zone then becomes the strongest contribution during the subgiant phase and the RGB as the density at the convective–radiative interface increases. For similar reasons, we also find that the dissipation of a metal-poor star is stronger than the dissipation of a metal-rich star during the PMS, the subgiant phase, and the RGB. The opposite trend is observed during the MS. Finally, we show that the contribution of a convective core for the most massive solar-type stars is negligible compared to that of the envelope because the mass distribution of the core does not favor the dissipation of tidal gravity waves.

**Key words.** planet–star interactions – planetary systems – stars: evolution – waves – hydrodynamics

## 1. Introduction

About 46% of the observed exoplanets are located within 20 times the radius of their host star (according to the database [exoplanet.eu](http://exoplanet.eu)<sup>1</sup>, e.g., [Schneider et al. 2011](#)). This configuration leads to significant star–planet interactions that affect the dynamics of these compact systems ([Cuntz et al. 2000](#)). The study of these interactions is therefore crucial for understanding the population of currently observed planetary systems and their evolution. The study of the orbital architecture of exosystems then improves our understanding of these processes and constrains the evolution models we rely on. The secular evolution of a star–planet system is essentially driven by stellar tides ([Leconte et al. 2010](#)), unless star–planet magnetic interactions develop due to the motion of the planet in the ambient magnetized stellar wind, which may have a significant role in the evolution of the system

([Strugarek et al. 2014, 2015, 2017](#)). In particular, the dissipation of tides in the host star, by ensuring angular momentum exchanges between the star rotation and the planetary orbit, is thought to play a major role in the secular evolution of orbital architecture ([Bolmont & Mathis 2016](#); [Benbakoura et al. 2019](#)) and star–planet obliquity ([Lai 2012](#); [Damiani & Mathis 2018](#)). Furthermore, as the reservoir of angular momentum of the planet is smaller than the one in its orbit, the planet tends to be synchronized within a few thousand years.

The gravitational response of the star to the planet leads to two types of flows: the non-wave-like equilibrium tide ([Zahn 1966](#); [Remus et al. 2012](#); [Ogilvie 2013](#)), which consists of the displacement induced by the hydrostatic adjustment of the stellar structure, and the dynamical tide, which corresponds to tidally forced internal waves. In stellar convective zones, the dynamical tide is constituted by inertial waves, restored by the Coriolis force, and is dissipated by the turbulent friction applied by the convection on tidal waves ([Ogilvie & Lin 2004, 2007](#)). The induced tidal dissipation may vary over several orders of

<sup>1</sup> <http://www.exoplanet.eu>, the database was consulted on December 18, 2020 to provide this estimate.

magnitude with tidal frequency, stellar mass, age, rotation, and metallicity (Mathis 2015; Gallet et al. 2017; Bolmont et al. 2017). When inertial waves are likely to be excited, that is, when the tidal frequency ranges between  $[-2\Omega_*, 2\Omega_*]$ ,  $\Omega_*$  being the stellar rotation angular velocity, this dissipation is several orders of magnitude higher than the dissipation of the equilibrium tide (Ogilvie & Lin 2007).

To obtain a complete picture of tidal dissipation in stars, we also need to consider the dynamical tide in stellar radiative zones (we refer to Ogilvie 2014 and Mathis 2019 for extensive reviews), which may compete with the dissipation in convective layers (Ivanov et al. 2013). Zahn (1970, 1975) first highlighted this process as a key dissipation mechanism in early-type stars to account for the circularization of massive close binaries (Zahn 1977; Savonije & Papaloizou 1983, 1984, 1997; Papaloizou & Savonije 1985, 1997; Savonije et al. 1995). This process occurs for  $a/R_* < 4$ ,  $a$  being the orbital semimajor axis and  $R_*$  the stellar radius (North & Zahn 2003). For the stars that have a convective core and a radiative envelope, the dissipation of gravity waves is more efficient than the dissipation of the equilibrium tide (Zahn 1977). Goodman & Dickson (1998) and Terquem et al. (1998) adopted a similar approach in the case of solar-type stars and showed that the resonant excitation of  $g$ -modes can compete with the dissipation of the equilibrium tide in the envelope. This effect has also been obtained in the case of gravito-inertial waves for uniformly rotating stars (Ogilvie & Lin 2007; Chernov et al. 2013; Ivanov et al. 2013).

Goldreich & Nicholson (1989) first proposed a physical interpretation of the dynamical tide in radiative zones. Internal gravity waves are excited near the convective-radiative interfaces by the tidal potential, where the buoyancy frequency matches the tidal frequency. They then propagate into the radiative zone, where they are damped by radiative diffusion (Zahn 1975, 1977), critical layers (Alvan et al. 2013), or nonlinear breaking (Goodman & Dickson 1998; Barker & Ogilvie 2010; Barker 2011; Guillot et al. 2014). In addition, the evanescent tail of the waves is subject to the friction applied by turbulent convection, which is commonly modeled with an eddy viscosity (Terquem et al. 1998). There, they deposit their angular momentum and thus alter the dynamics of the system considered. In particular, when we consider an early-type star with a radial differential rotation in its radiative zone, this process leads to a synchronization of the star starting from its surface (Goldreich & Nicholson 1989).

The main dependences of the torque induced by the dissipation of tidal gravity waves are well understood. In particular, the location and stellar properties at the interface between the convective and radiative zones are critical parameters for estimating the amplitude of the dissipation. However, the effective contribution of the tidal forcing to the gravity-wave torque requires an intensive investigation of forced oscillations. As was pointed out by Kushnir et al. (2017), this factor has been studied independently for early-type stars in the context of binary systems (e.g., Zahn 1975; Goldreich & Nicholson 1989) and late-type stars in the framework of the secular evolution of exoplanetary systems (e.g., Goodman & Dickson 1998; Terquem et al. 1998). In order to track the fate of the system from the birth of the star until its death, we need a unified formalism allowing us to take any changes in stellar structure during the evolution into account.

In this context, the effect of stellar structure and evolution, which is subject to complex variations over time (Kippenhahn & Weigert 1994), on the tidal dissipation in radiative zones constitutes a key issue that needs to be addressed. Barker (2020) carried out a first study of tidal dissipation through gravity

waves during stellar evolution. In the context of the evolution of planetary systems, he compared the dissipation in the stellar radiative zone with the frequency-averaged dissipation through inertial waves in the stellar convective zone for a given stellar rotation period and orbital period. He reported that the dissipation of tidal gravity waves is the dominant mechanism for the migration of close-in planets. This may also be a way to account for the survival of close-in exoplanets, depending on the host star properties (Barker & Ogilvie 2010; Guillot et al. 2014).

Furthermore, tidal dissipation for a trilayer structure, for example, in the case of F-type stars and red giants in the red clump should be studied. It can be very important for our understanding of binaries and planetary systems because in these configurations, the dissipation of the dynamical tide in the convective zone is weaker than the dissipation of the equilibrium tide (Mathis 2015; Gallet et al. 2017; Beck et al. 2018). Some aspects of this question have been extensively studied by Fuller (2017), who assessed the tidal dissipation through standing  $g$ -modes in the case of F- and A-type stars by taking resonance locking into account.

The goal of our work is to provide a general formalism to assess tidal dissipation in stellar radiative zones that may be applicable to late- and early-type stars as well as to trilayer structures. On this basis, we investigate the effect of stellar structure and evolution on tidal dissipation for low-mass stars and study the contribution of a convective core for F-type stars. In Sect. 2, we study the forced adiabatic oscillations in a spherical geometry. From there, we compute in Sect. 3 the energy flux that is carried by the waves and the induced tidal torque. In Sect. 4 we apply our formalism to massive stars that match the Zahn (1975) formulation and to low-mass stars. In Sect. 5, we investigate the effect of stellar structure and evolution on tidal dissipation in low-mass stars. For F-type stars, we simultaneously evaluate the contributions of the convective core and envelope to the dynamical tide. All of these results are then summarized and discussed, and we present perspectives in Sect. 6.

## 2. Forced adiabatic oscillations in a spherical geometry

### 2.1. Statement of the problem

We aim to evaluate the tidal dissipation in stellar radiative zones driven by internal gravity waves (IGW). To this end, we modeled the stellar interior as an inviscid fluid. For instance, the Sun has a Prandtl number of about  $3 \times 10^{-6}$  (Brun & Zahn 2006), meaning that thermal diffusion dominates viscosity effects.

To account for the interior of early- and late-type stars, we considered a convective layer delimited by the radii  $r_{\text{conv}}$  and  $r_{\text{int}}$ , where the interface of the convective to the radiative zone is located. A radiative shell is then delimited by the radii  $r_{\text{int}}$  and  $r_{\text{rad}}$ . In a solar-type star configuration, the waves are launched near the base of the convective envelope. Then energy propagates inward to the center before the waves dissipate (see the left panel in Fig. 1), whereas in the massive star configuration, energy is transported outward to the stellar surface (see the right panel in Fig. 1). To take this changing direction of propagation into account, we defined  $\epsilon = \text{sign}(r_{\text{conv}} - r_{\text{rad}})$ . This quantity is equal to 1 for an inward energy transport through gravity waves and equal to  $-1$  otherwise. The values of  $r_{\text{rad}}$ ,  $r_{\text{conv}}$ , and  $\epsilon$  for massive and solar-type stars are listed in Table 1.

We focus on the progressive low-frequency waves that are damped most strongly (e.g., Press 1981; Zahn et al. 1997; Alvan et al. 2015). Terquem et al. (1998) have shown that the excitation

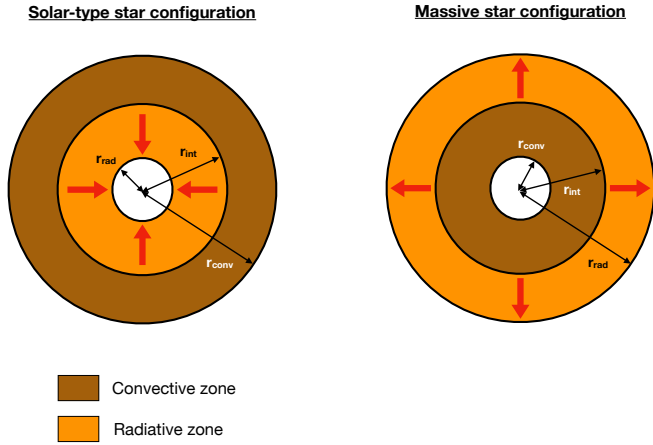


**Fig. 1.** Configurations of the radiative and convective spherical shells in our work. In brown we show the convective layer. In orange we plot the radiative layer. The red arrows represent the energy flux carried by tidal gravity waves.

**Table 1.** Values of  $r_{\text{rad}}$ ,  $r_{\text{conv}}$ , and  $\epsilon$  for massive and solar-type stars.

Type of star	$r_{\text{rad}}$	$r_{\text{conv}}$	$\epsilon$
Massive	$R_*$	0	-1
Solar-type	0	$R_*$	1

of a fixed spectrum of  $g$ -modes, dissipated by radiative damping, does not affect the secular evolution of the system. In our model, the progressive gravity waves deposit angular momentum at the place they are damped, which drives spin-orbit angular momentum exchanges and the evolution of the system.

Following [Alvan et al. \(2015\)](#), we first assessed the cutoff frequency that separates progressive waves and  $g$ -modes. During their propagation, gravity waves are subject to radiative damping, which in the quasi-adiabatic regime for low-frequency waves results in an amplitude of the wave damped by a factor  $\exp(-\tau/2)$  where

$$\tau(r, l, \omega) = \epsilon [l(l+1)]^{\frac{3}{2}} \int_r^{r_{\text{int}}} K_T \frac{N^3}{\omega^4 r_1^3} dr_1, \quad (1)$$

with  $K_T$  the thermal diffusivity of the medium (we refer to [Zahn et al. 1997](#), for more details). In order to separate standing modes and progressive waves, we assume that a stationary wave can form if

$$\tau(r_{\text{rad}}, l, \omega) \leq 1. \quad (2)$$

In this case, the amplitude of the waves is sufficient at  $r = r_{\text{rad}}$  for them to undergo reflection, leading to the formation of a standing  $g$ -mode. This condition defines the cutoff frequency  $\omega_c$  as

$$\omega \geq [l(l+1)]^{\frac{3}{2}} \left( \epsilon \int_{r_{\text{rad}}}^{r_{\text{int}}} K_T \frac{N^3}{r_1^3} dr_1 \right)^{\frac{1}{4}} \equiv \omega_c, \quad (3)$$

above which standing modes form, as shown in [Fig. 2](#). For frequencies higher than  $\omega_c$ , gravity waves carry enough energy to undergo a reflection in spite of radiative damping, allowing the generation of individual modes. Below this frontier (in blue in

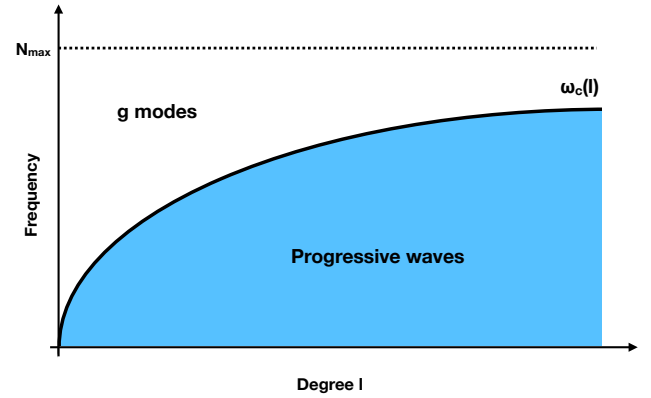


**Fig. 2.** Nature of internal gravity waves as a function of degree  $l$  and frequency. The dashed black line corresponds to the maximum value of the Brunt-Väisälä frequency  $N_{\text{max}}$  in the radiative zone. The black line corresponds to the cutoff frequency  $\omega_c$  as a function of the degree, marking the separation between standing  $g$ -modes (in white, above) and progressive internal gravity waves (in blue, below).

[Fig. 2](#)), waves are sufficiently damped to prevent standing modes from forming. The spectrum is then only composed of progressive waves. Because propagative waves are damped at a distance that is smaller than the size of the radiative zone, all the energy carried by gravity waves is therefore dissipated inside the star before any reflection. This configuration leads to the most efficient dissipation if no critical layer or nonlinear effect is taken into account.

However, a tidal gravity wave is likely to transfer its entire angular momentum to the star through other dissipation mechanisms. If the amplitude of the wave exceeds a critical value the case of a low-mass star, it can break near the center of the star, thus transferring its angular momentum to the mean flow and bringing the central regions of the star into corotation with the tidal forcing ([Barker & Ogilvie 2010](#); [Barker 2011](#)). A similar process occurs near the stellar surface in the case of intermediate-mass and massive stars ([Rogers et al. 2013](#)). This forms a critical layer that acts as an absorbent barrier for the subsequent waves. This process occurs if the planetary mass exceeds a critical value that decreases sharply with stellar mass and stellar age ([Barker 2020](#)) as the strength of the stratification increases. We provide a similar wave-braking criterion in [Appendix D](#). For stellar masses higher than  $0.9 M_{\odot}$ , the minimum planetary mass required to induce wave braking may fall below 1 Jupiter mass at ages younger than 10 Gyr. Moreover, the interaction of tidal gravity waves with the differential rotation of the surrounding fluid may lead to the formation of a critical layer when the frequency of excited waves is on the same order of magnitude as the angular velocity of the fluid. In the radiative zone of solar-type stars, the fluid remains stable in this configuration, and the amplitude of gravity waves is damped by the critical layer ([Alvan et al. 2013](#)). For a mode of azimuthal number  $m$  at an orbital harmonic  $N$ , this layer exists at a radius  $r_{\text{CL}}$  in an inertial reference frame if

$$\omega = m \Omega_{\text{RZ}}(r_{\text{CL}}), \quad (4)$$

where  $\Omega_{\text{RZ}}(r_{\text{CL}})$  is the angular velocity of the radiative zone at the radius  $r_{\text{CL}}$ . As  $\omega = N n_{\text{orb}}$  in an inertial reference frame, with  $n_{\text{orb}}$  the mean motion of the planetary orbit, this leads to  $\Omega_{\text{RZ}}(r) = N/m n_{\text{orb}}$ . We can assess the range of orbital periods leading to a potential interaction with a critical layer by considering a coplanar and circular planetary orbit ( $N = m = 2$ ). The

radiative core of a solar-type star tends to synchronize its spin with that of the convective zone during the MS (e.g., [Gallet & Bouvier 2015](#); [Benomar et al. 2015](#)). Therefore we assumed a weak differential rotation within the star as a first approximation. Thus we can provide an upper bound of the orbital period required for the creation of a critical layer by focusing on the evolution of the surface rotation rate of the star (which is also the rotation rate of the convective envelope when we assume that the latter is in solid-body rotation). An interaction between a tidal gravity wave and a critical layer may therefore occur within a solar-type star if the orbital period of the planet is shorter than 10 days during the PMS and shorter than 50 days during the MS (we refer to [Gallet & Bouvier 2015](#); [Amard et al. 2016](#), for more details about the rotational evolution of the radiative zone of solar-type stars).

In order to account for all these cases for which tidal dissipation is likely to be effective, we assume in our model that all the energy carried by gravity waves is dissipated inside the star before any reflection. In this way, we may be able to provide an upper bound of tidal dissipation and to unravel the effect of the stellar internal structure and rotation. In this context, we consider forced adiabatic oscillations in the stellar interior. The tidal torque is directly inferred from the angular momentum flux carried by the internal gravity waves.

## 2.2. Forced dynamics of internal gravity waves

We assumed that the star is in hydrostatic equilibrium, which leads to

$$\nabla p_0 = -\rho_0 \mathbf{g}_0, \quad (5)$$

where  $p_0$  is the pressure inside the star,  $\rho_0$  is its local density, and  $\mathbf{g}_0$  is the gravity. The subscript 0 in these quantities refers to the unperturbed background. This structure is then perturbed by the tidal potential  $U_T$  applied by the companion. By introducing velocity ( $\mathbf{v}_1$ ), pressure ( $p_1$ ), and gravitational potential ( $\varphi_1$ ) perturbations induced by the planet, we can linearize the equations of hydrodynamics around the equilibrium state in this approach by ignoring all dissipative mechanisms:

$$\begin{cases} \partial_t \rho_1 + \mathbf{v}_1 \cdot \nabla \rho_0 + \rho_0 \nabla \cdot \mathbf{v}_1 = 0 \\ \partial_t \mathbf{v}_1 = -\frac{1}{\rho_0} \nabla p_1 + \frac{\rho_1}{\rho_0^2} \nabla p_0 - \nabla \varphi_1 - \nabla U_T \\ \frac{1}{\rho_0} [\partial_t p_1 + (\mathbf{v}_1 \cdot \nabla) p_0] - \frac{\Gamma_1}{\rho_0} [\partial_t \rho_1 + (\mathbf{v}_1 \cdot \nabla) \rho_0] = 0, \end{cases} \quad (6)$$

with  $\Gamma_1 = (\partial \ln p_0 / \partial \ln \rho_0)_S$  the adiabatic exponent of the fluid, and  $S$  is the specific macroscopic entropy. We made use of the spherical coordinates  $(r, \theta, \varphi)$ , with  $r$  the radial coordinate,  $\theta$  the colatitude, and  $\varphi$  the longitude, and their corresponding unit-vector basis  $(\mathbf{e}_r, \mathbf{e}_\theta, \mathbf{e}_\varphi)$ . After introducing the Lagrangian displacement field  $\xi$ , we developed all the fluctuations on the spherical harmonics  $Y_l^m(\theta, \varphi) \propto P_l^m(\cos \theta) e^{im\varphi}$  as follows:

$$\xi(r, \theta, \varphi, t) = \sum_{l,m} [\xi_{r;l,m}(r) Y_l^m(\theta, \varphi) \mathbf{e}_r + \xi_{h;l,m}(r) \nabla_h Y_l^m(\theta, \varphi)] e^{-i\omega t}, \quad (7)$$

$$\rho_1(r, \theta, \varphi, t) = \sum_{l,m} \tilde{\rho}_{l,m}(r) Y_l^m(\theta, \varphi) e^{-i\omega t}, \quad (8)$$

$$p_1(r, \theta, \varphi, t) = \sum_{l,m} \tilde{p}_{l,m}(r) Y_l^m(\theta, \varphi) e^{-i\omega t}, \quad (9)$$

$$\varphi_1(r, \theta, \varphi, t) = \sum_{l,m} \tilde{\varphi}_{l,m}(r) Y_l^m(\theta, \varphi) e^{-i\omega t}, \quad (10)$$

$$U_T(r, \theta, \varphi, t) = \sum_{l,m} \varphi_{T;l,m}(r) Y_l^m(\theta, \varphi) e^{-i\omega t}, \quad (11)$$

with  $\nabla_h = \partial_\theta \mathbf{e}_\theta + (1/\sin \theta) \partial_\varphi \mathbf{e}_\varphi$  the horizontal gradient. We focus on the behavior of a single mode in the remaining work, and we assume that  $l$  and  $m$  are fixed by the tidal potential (e.g.,  $l = m = 2$  in a coplanar configuration,  $l = 2$  and  $m = 0$  for eccentricity tides,  $l = 2$  and  $m = 1$  for obliquity tides). For the sake of simplicity, the degree and order dependencies of the components of each perturbed quantity are therefore no longer specified. For instance, we write  $\xi_r$  instead of  $\xi_{r;l,m}$ .

Furthermore, we adopted the Cowling approximation ([Cowling 1941](#)), where we neglected the fluctuations of the gravific potential of the wave. This approximation is well justified for low-frequency waves. This leads to ([Press 1981](#); [Auclair-Desrotour et al. 2017](#))

$$\begin{cases} \partial_r (r^2 \xi_r) + \frac{\partial_r p_0}{\Gamma_1 p_0} (r^2 \xi_r) = \left( \frac{l(l+1)}{\omega^2} - \frac{\rho_0 r^2}{\Gamma_1 p_0} \right) y + \frac{l(l+1)}{\omega^2} \varphi_T \\ \partial_r y - y \frac{N^2}{g_0} = \frac{1}{r^2} (\omega^2 - N^2) (r^2 \xi_r) - \partial_r \varphi_T, \end{cases} \quad (12)$$

where we have introduced the reduced pressure  $y = \tilde{p}/\rho_0$  and the Brunt–Väisälä frequency  $N^2 = g_0 \left( \frac{\partial_r p_0}{\Gamma_1 p_0} - \frac{\partial_r \rho_0}{\rho_0} \right)$ .

In order to reunite the [Zahn \(1975\)](#), [Goldreich & Nicholson \(1989\)](#), [Goodman & Dickson \(1998\)](#), and [Barker & Ogilvie \(2010\)](#) prescriptions, among others, in a flexible framework allowing for the study of a given system dynamics throughout stellar evolution, we carried out and present in this paper all the necessary derivations.

## 2.3. Wave behavior in the radiative zone

We now aim to study the propagation of tidal gravity waves within the stellar interior. To do so, we first focus on the behavior of these waves in the radiative zone of the star.

### 2.3.1. Approximations in the radiative zone

Following [Press \(1981\)](#), in the stably stratified radiative zone, where  $N^2 > 0$ , deriving the first equation of (12) with respect to  $r$  and including the second equation gives

$$\partial_{rr} (r^2 \xi_r) + \frac{\partial_r p_0}{\rho_0} \partial_r (r^2 \xi_r) + \mathcal{K} r^2 \xi_r = \mathcal{A} + \mathcal{F}_T, \quad (13)$$

with

$$\begin{aligned} \mathcal{K} &= \left( \frac{N^2}{\omega^2} - 1 \right) \frac{l(l+1)}{r^2} + \partial_r \left( \frac{\partial_r p_0}{\Gamma_1 p_0} \right), \\ \mathcal{F}_T &= -\frac{l(l+1)}{\omega^2} \left( \frac{l(l+1)}{\omega^2} - \frac{\rho_0 r^2}{\Gamma_1 p_0} \right)^{-1} \frac{N^2}{g_0} \varphi_T, \\ \mathcal{A} &= \partial_r (r^2 \xi_r) \frac{N^2}{g_0} \left[ \frac{l(l+1)}{\omega^2} \left( \frac{l(l+1)}{\omega^2} - \frac{\rho_0 r^2}{\Gamma_1 p_0} \right)^{-1} - 1 \right] \\ &\quad + (r^2 \xi_r) \left[ \frac{l(l+1)}{\omega^2} \left( \frac{l(l+1)}{\omega^2} - \frac{\rho_0 r^2}{\Gamma_1 p_0} \right)^{-1} \frac{N^2}{g_0} \frac{\partial_r p_0}{\Gamma_1 p_0} \right] - \partial_r \left[ \frac{\rho_0 r^2}{\Gamma_1 p_0} y \right], \end{aligned} \quad (14)$$

where the last term in  $\mathcal{A}$  can be replaced through Eq. (12). By using the anelastic approximation to filter out acoustic waves, we can assume that

$$\frac{\rho_0 r^2}{\Gamma_1 p_0} \ll \frac{l(l+1)}{\omega^2}. \quad (15)$$

Therefore, we can simplify the expression of  $\mathcal{A}$  as

$$\mathcal{A} \approx -\xi_r \frac{N^2 r^2}{c_s^2} - \partial_r \left[ \frac{r^2 y}{c_s^2} \right], \quad (16)$$

with  $c_s = \sqrt{\Gamma_1 p_0 / \rho_0}$  the speed of sound. In the anelastic approximation, terms of order  $1/c_s^2$  (Spiegel & Veronis 1960) are neglected, which leads to the simplified relation

$$\partial_{rr} (r^2 \xi_r) + \partial_r (r^2 \xi_r) \frac{\partial_r \rho_0}{\rho_0} + \mathcal{K} r^2 \xi_r = -\frac{N^2}{g_0} \varphi_T. \quad (17)$$

To obtain a Schrödinger-like equation in the radiative zone, we introduce a new function  $\psi(r) = \rho_0^{\frac{1}{2}} r^2 \xi_r$ , which leads to

$$\frac{d^2 \psi}{dr^2} + \frac{l(l+1)}{r^2} \left( \frac{N^2}{\omega^2} - 1 \right) \psi = \frac{l(l+1)N^2}{\omega^2 r^2} \left( -\rho_0^{\frac{1}{2}} r^2 \frac{\varphi_T}{g_0} \right) + \mathcal{V}, \quad (18)$$

with  $\mathcal{V} = \psi \left[ \rho_0^{-\frac{1}{2}} \partial_{rr} (\rho_0^{\frac{1}{2}}) - \partial_r \left( \frac{\partial_r \rho_0}{\Gamma_1 p_0} \right) \right] \sim L^{-2} \psi$ , given a characteristic length  $L$  of our system. Equations (17) and (18) are equivalent to the Zahn (1975), Savonije & Papaloizou (1984) and Goodman & Dickson (1998) formulations, whose main discrepancies come from the terms taken into account in  $\mathcal{V}$ . Here, we assumed that the characteristic length of variation of the background is large compared the wavelength of a gravity wave, that is,

$$\left( \frac{N^2}{\omega^2} - 1 \right) \frac{l(l+1)}{r^2} \gg L^{-2}. \quad (19)$$

Therefore, we can neglect the  $\mathcal{V}$  term and obtain the equation ruling the behavior of internal gravity waves in the radiative zone (Zahn 1975),

$$\psi'' + \frac{l(l+1)}{r^2} \left( \frac{N^2}{\omega^2} - 1 \right) \psi = \frac{l(l+1)N^2}{\omega^2 r^2} \left( -\rho_0^{\frac{1}{2}} r^2 \frac{\varphi_T}{g_0} \right), \quad (20)$$

where for an arbitrary quantity  $F$ ,  $F' = \frac{dF}{dr}$ . This convention is used in the remainder of this work to simplify the notations.

### 2.3.2. Solutions in the radiative zone

We now have to solve Eq. (20) in the radiative zone. Far from the interface, we can assume that  $N^2 \gg \omega^2$  because we consider low-frequency waves. Then we can use the WKBJ approximation (Fröman & Fröman 1965), and the solution becomes

$$\psi(r) = -\rho_0^{\frac{1}{2}} r^2 \frac{\varphi_T}{g_0} + C_W \frac{1}{\sqrt{k_r}} e^{\epsilon i(\tau_W - \tau_0)}, \quad (21)$$

where  $k_r = \sqrt{\left( \frac{N^2}{\omega^2} - 1 \right) \frac{l(l+1)}{r^2}}$  is the radial wavenumber,  $C_W$ ,  $\tau_0$  are constants and  $\tau_W = \epsilon \int_{r_{\text{rad}}}^r k_r(r) dr$ . The factor  $\epsilon$  is equal to 1 for an inward transport of energy through gravity waves and equal to  $-1$  otherwise.

Furthermore, a turning point occurs near the radiative-convective interface, where  $N \approx \omega$ . The WKBJ approximation is no longer relevant, and we expand the square of the Brunt-Väisälä frequency around the interface  $r = r_{\text{int}}$  as

$$N^2 = \omega^2 + \left| \frac{dN^2}{dr} \right|_{\text{int}} \epsilon (r_{\text{int}} - r). \quad (22)$$

Equation (20) now becomes an inhomogeneous Airy equation (Zahn 1975; Goodman & Dickson 1998):

$$\frac{d^2 \psi}{d\eta^2} + v^2 \eta \psi = \frac{l(l+1)N^2}{\omega^2 r^2} \left( -\rho_0^{\frac{1}{2}} r^2 \frac{\varphi_T}{g_0} \right), \quad (23)$$

with

$$v^2 = \frac{l(l+1)}{r_{\text{int}}^2 \omega^2} \left| \frac{dN^2}{dr} \right|_{\text{int}}, \quad (24)$$

$$\eta = \epsilon (r_{\text{int}} - r). \quad (25)$$

The solution  $\psi_h$  of the corresponding homogenous equation can be written as a linear combination of the Airy functions Ai and Bi as follows (Abramowitz & Stegun 1972):

$$\psi_h(\eta) = C_A \text{Ai} \left[ v^{\frac{2}{3}} (-\eta) \right] + C_B \text{Bi} \left[ v^{\frac{2}{3}} (-\eta) \right], \quad (26)$$

where  $C_A$  and  $C_B$  are two constants. Furthermore, the Airy functions can be linked to the Bessel functions  $J_{\frac{1}{3}}$  and  $J_{-\frac{1}{3}}$  as

$$\text{Ai}(-x) = \frac{\sqrt{x}}{3} \left[ J_{\frac{1}{3}} \left( \frac{2}{3} x^{\frac{3}{2}} \right) + J_{-\frac{1}{3}} \left( \frac{2}{3} x^{\frac{3}{2}} \right) \right], \quad (27)$$

$$\text{Bi}(-x) = \sqrt{\frac{x}{3}} \left[ J_{-\frac{1}{3}} \left( \frac{2}{3} x^{\frac{3}{2}} \right) - J_{\frac{1}{3}} \left( \frac{2}{3} x^{\frac{3}{2}} \right) \right]. \quad (28)$$

We rely for the remainder of this work on a formulation based on Bessel functions, which allows us to link the Zahn (1970, 1975) and Ivanov et al. (2013) approaches, and to simplify the matching of the different solutions. The solution  $\psi_h$  therefore becomes

$$\psi_h(\tau) = \left( \frac{\tau}{2} \right)^{\frac{1}{3}} \left[ \alpha_{\text{rad}} J_{\frac{1}{3}}(\tau) + \beta_{\text{rad}} J_{-\frac{1}{3}}(\tau) \right], \quad (29)$$

with  $\tau = \frac{2}{3} v \eta^{\frac{3}{2}}$ ,  $\alpha_{\text{rad}} = C_A \cdot 3^{-\frac{2}{3}} - C_B \cdot 3^{-\frac{1}{6}}$  and  $\beta_{\text{rad}} = C_A \cdot 3^{-\frac{2}{3}} + C_B \cdot 3^{-\frac{1}{6}}$ . A particular solution  $\psi_p$  of the inhomogeneous Airy equation, vanishing at the interface, can be expressed as (see Appendix A)

$$\psi_p(\eta) = Z(\eta) + \left( \frac{\tau}{2} \right)^{\frac{1}{3}} \left[ \alpha_{\text{rad,p}} J_{\frac{1}{3}}(\tau) + \beta_{\text{rad,p}} J_{-\frac{1}{3}}(\tau) \right], \quad (30)$$

where  $Z(\eta) = -\rho_0^{\frac{1}{2}} r^2 \frac{\varphi_T}{g_0}$  is the particular solution of Eq. (20) in the WKBJ formulation associated with the equilibrium tide,  $\alpha_{\text{rad,p}} = -\frac{dZ}{d\eta}(0) \left( \frac{v}{3} \right)^{-\frac{2}{3}} \Gamma\left(\frac{4}{3}\right)$  and  $\beta_{\text{rad,p}} = -Z(0) \Gamma\left(\frac{2}{3}\right)$ . Because

$J_{\pm\frac{1}{3}}(\tau) \underset{\tau \rightarrow +\infty}{\sim} \sqrt{\frac{2}{\pi\tau}} \cos\left(\tau \mp \frac{\pi}{6} - \frac{\pi}{4}\right)$  far from the interface, the particular solution obtained with the Bessel formulation matches the particular solution derived through the WKBJ approximation.

## 2.4. Wave behavior in the convective zone

In the previous section we studied the propagation of tidal gravity waves in the radiative zone. We now derive the equations governing the behavior of such waves in the convective zone of the star and solve them formally.

### 2.4.1. Approximations in the convective zone

In the convective zone, we assumed  $N^2 = 0$  because we consider adiabatic oscillations. This approximation holds in convective cores and in the regions of convective envelopes for which convection is efficient (at radii up to  $0.9 R_*$ , below the superadiabatic layer; we refer to [Lebreton et al. 2014](#)). In this configuration, Eqs. (12) become

$$\begin{cases} \partial_r (r^2 \xi_r) = -\frac{\partial_r p_0}{\Gamma_1 p_0} (r^2 \xi_r) + \frac{\rho_0 r^2}{\Gamma_1 p_0} (\varphi_T - \chi) + \frac{l(l+1)}{\omega^2} \chi \\ \xi_r = \frac{\partial_r \chi}{\omega^2}, \end{cases} \quad (31)$$

where we define  $\chi = y + \varphi_T$ . Because  $N^2 = 0$ , we have  $\frac{\partial_r p_0}{\Gamma_1 p_0} = \frac{\partial_r \rho_0}{\rho_0}$ , which leads to

$$\begin{cases} \partial_r (r^2 \xi_r) = -\frac{\partial_r \rho_0}{\rho_0} (r^2 \xi_r) + \frac{\rho_0 r^2}{\Gamma_1 p_0} (\varphi_T - \chi) + \frac{l(l+1)}{\omega^2} \chi \\ \xi_r = \frac{\partial_r \chi}{\omega^2} \end{cases}. \quad (32)$$

As we focus on low-frequency gravity waves, we rely on the anelastic approximation, which gives

$$\partial_r (r^2 \xi_r) = -\frac{\partial_r \rho_0}{\rho_0} (r^2 \xi_r) + \frac{l(l+1)}{\omega^2} \chi + z \quad (33)$$

with  $z = -\frac{\partial_r \rho_0}{\rho_0} \frac{r^2 \varphi_T}{g_0}$ . We now define the quantity  $X(r) = \rho_0 r^2 \xi_r$ , which verifies the following relation:

$$X' = \frac{l(l+1)}{\omega^2} \rho_0 \chi + \rho_0 z. \quad (34)$$

By differentiating Eq. (34), we derive the equation ruling the behavior of evanescent internal gravity waves in the convective zone ([Zahn 1975](#); [Ivanov et al. 2013](#)),

$$X'' - \frac{\partial_r \rho_0}{\rho_0} X' - \frac{l(l+1)}{r^2} X = \rho_0 z'. \quad (35)$$

### 2.4.2. Solutions in the convective zone

We now need to solve Eq. (35) in the convective zone. Following [Zahn \(1975\)](#), when we consider  $X_1$ ,  $X_2$  two independent solutions of the corresponding homogeneous ordinary differential equation, the general solution of Eq. (35) can be written as

$$X = \left[ C_1 - \int_{r_{\text{conv}}}^r \Lambda^{-1} \rho_0 z' X_2 dr \right] X_1 + \left[ C_2 + \int_{r_{\text{conv}}}^r \Lambda^{-1} \rho_0 z' X_1 dr \right] X_2, \quad (36)$$

where  $C_1$  and  $C_2$  are two constants of integration, and  $\Lambda = X_2' X_1 - X_1' X_2$  is their Wronskian. When we consider the displacement functions  $\xi_1 = X_1 / (\rho_0 r^2)$ ,  $\xi_2 = X_2 / (\rho_0 r^2)$  and their

Wronskian  $\Lambda_\xi = \xi_1 \xi_2' - \xi_2 \xi_1'$ , the particular solution of Eq. (35) can be written in an alternative form, knowing that  $\Lambda \propto \rho_0$ ,

$$\int_{r_{\text{conv}}}^r \Lambda^{-1} \rho_0 z' X_i dr = \Lambda_\xi^{-1} (r_{\text{int}}) r_{\text{int}}^{-2} \xi_i (r_{\text{int}}) \int_{r_{\text{conv}}}^r z' \frac{X_i}{X_i(r_{\text{int}})} dr, \quad (37)$$

with  $i = 1$  or  $2$ . Furthermore, the integral appearing in Eq. (37) can be expressed as

$$\int_{r_{\text{conv}}}^r z' X_i dr = \mathcal{B} + \mathcal{F}_i, \quad (38)$$

with

$$\begin{aligned} \mathcal{B} &= \left[ -\left\{ \frac{\rho_0'}{\rho_0} \frac{r^2 \varphi_T}{g_0} + \left( \frac{r^2 \varphi_T}{g_0} \right)' \right\} X_i + \left( \frac{r^2 \varphi_T}{g_0} \right) X_i' \right]_{r_{\text{conv}}}^r, \\ \mathcal{F}_i &= \int_{r_{\text{conv}}}^r \left[ \left( \frac{r^2 \varphi_T}{g_0} \right)'' - \frac{l(l+1)}{r^2} \left( \frac{r^2 \varphi_T}{g_0} \right) \right] X_i dr. \end{aligned} \quad (39)$$

## 2.5. Matching of the solutions

We have determined the functions describing the forced adiabatic oscillations in the radiative zone and the convective zone. We now need to match the different solutions obtained in order to describe the behavior of tidal gravity waves in the whole stellar interior.

### 2.5.1. Matching the radiative-convective zone

At the interface, we match the solutions in the radiative and convective layers by taking tidal forcing into account.

For the sake of simplicity, we define  $S_+(\tau) = \left(\frac{\tau}{2}\right)^{\frac{1}{3}} J_{\frac{1}{3}}(\tau)$  and  $S_-(\tau) = \left(\frac{\tau}{2}\right)^{\frac{1}{3}} J_{-\frac{1}{3}}(\tau)$ , which constitute a basis for the homogeneous solution in the radiative zone in a Bessel formulation. Near the interface, we can express a basis solution of the homogeneous equation in the convective zone  $\rho_0^{-\frac{1}{2}} X_i$ , with  $i = 1$  or  $2$ , as a linear combination  $\alpha_i S_+ + \beta_i S_-$ . In this way, we obtain

$$\rho_0^{-\frac{1}{2}} X(r_{\text{int}}) = (\alpha_{\text{conv}} + \alpha_{\text{conv,p}}) S_+(0) + (\beta_{\text{conv}} + \beta_{\text{conv,p}}) S_-(0), \quad (40)$$

where

$$\begin{cases} \alpha_{\text{conv}} = \alpha_1 C_1 + \alpha_2 C_2 \\ \beta_{\text{conv}} = \beta_1 C_1 + \beta_2 C_2 \\ \alpha_{\text{conv,p}} = -\alpha_1 \int_{r_{\text{conv}}}^{r_{\text{int}}} \Lambda^{-1} \rho_0 z' X_2 dr + \alpha_2 \int_{r_{\text{conv}}}^{r_{\text{int}}} \Lambda^{-1} \rho_0 z' X_1 dr \\ \beta_{\text{conv,p}} = -\beta_1 \int_{r_{\text{conv}}}^{r_{\text{int}}} \Lambda^{-1} \rho_0 z' X_2 dr + \beta_2 \int_{r_{\text{conv}}}^{r_{\text{int}}} \Lambda^{-1} \rho_0 z' X_1 dr. \end{cases} \quad (41)$$

Furthermore, we can choose  $\rho_0^{-\frac{1}{2}} X_2$  to match the basis solution  $S_+$  at the interface. Then we have  $\alpha_2 = 1$  and  $\beta_2 = 0$ . We can also assume that  $\alpha_{\text{conv}} \ll \beta_{\text{conv}}$  without restricting the generality of the foregoing, which amounts to choosing a solution  $X_1$  close to  $S_-$ . We now aim to characterize all the solutions at the interface and to better constrain the integration constants. To this end, we write  $S_+$  and  $S_-$  as

$$S_\pm(\tau) = \frac{1}{2} \left[ 3^{\frac{2}{3}} \text{Ai} \left( v^{\frac{2}{3}}(-\eta) \right) \mp 3^{\frac{1}{3}} \text{Bi} \left( v^{\frac{2}{3}}(-\eta) \right) \right], \quad (42)$$

which at the interface leads to

$$\begin{cases} S_+(0) = 0 \\ S_-(0) = \frac{1}{\Gamma\left(\frac{2}{3}\right)} \\ \partial_r S_+(0) = \frac{-\epsilon}{\Gamma\left(\frac{4}{3}\right)} \left(\frac{v}{3}\right)^{\frac{2}{3}} \\ \partial_r S_-(0) = 0. \end{cases} \quad (43)$$

On the basis of these calculations, the general solution  $X_h = \alpha_{\text{conv}} S_+ + \beta_{\text{conv}} S_-$  of the homogeneous equation in the convective zone verifies the following condition (Zahn 1975):

$$\frac{\alpha_{\text{conv}}}{\beta_{\text{conv}}} \frac{\Gamma\left(\frac{2}{3}\right)}{\Gamma\left(\frac{4}{3}\right)} \left(\frac{v}{3}\right)^{\frac{2}{3}} = -\epsilon \frac{\frac{d}{dr}(\rho_0^{-\frac{1}{2}} X_h)_{\text{int}}}{(\rho_0^{-\frac{1}{2}} X_h)_{\text{int}}}. \quad (44)$$

Moreover, in the same layer, the Wronskian  $\Lambda_\xi$  of the displacement functions corresponding to the basis solutions of the homogeneous equation can be expressed as

$$\begin{aligned} \Lambda_\xi(r_{\text{int}}) &= \rho_0^{-2}(r_{\text{int}}) r_{\text{int}}^{-4} [X_1(r_{\text{int}}) X_2'(r_{\text{int}}) - X_2(r_{\text{int}}) X_1'(r_{\text{int}})] \\ &= -\epsilon \rho_0^{-1}(r_{\text{int}}) r_{\text{int}}^{-4} \frac{\beta_1}{\Gamma\left(\frac{4}{3}\right) \Gamma\left(\frac{2}{3}\right)} \left(\frac{v}{3}\right)^{\frac{2}{3}}. \end{aligned} \quad (45)$$

The values of the displacement functions themselves at the interface  $\xi_i(r_{\text{int}}) = \rho_0^{-1}(r_{\text{int}}) r_{\text{int}}^{-2} X_i(r_{\text{int}})$  become

$$\xi_i(r_{\text{int}}) = \begin{cases} \rho_0^{-\frac{1}{2}}(r_{\text{int}}) r_{\text{int}}^{-2} \frac{\beta_1}{\Gamma\left(\frac{2}{3}\right)}, & \text{if } i = 1 \\ 0, & \text{if } i = 2. \end{cases} \quad (46)$$

Therefore we obtain from Eq. (37)

$$\int_{r_{\text{conv}}}^{r_{\text{int}}} \Lambda^{-1} \rho_0 z' X_1 dr = -\epsilon \rho_0^{\frac{1}{2}}(r_{\text{int}}) \Gamma\left(\frac{4}{3}\right) \left(\frac{v}{3}\right)^{-\frac{2}{3}} \int_{r_{\text{conv}}}^{r_{\text{int}}} z' \frac{X_1}{X_1(r_{\text{int}})} dr. \quad (47)$$

Then we have for the particular solution in the convective zone

$$\begin{aligned} \alpha_{\text{conv,p}} &= -\alpha_1 \int_{r_{\text{conv}}}^{r_{\text{int}}} \Lambda^{-1} \rho_0 z' X_2 dr \\ &\quad - \epsilon \rho_0^{\frac{1}{2}}(r_{\text{int}}) \Gamma\left(\frac{4}{3}\right) \left(\frac{v}{3}\right)^{-\frac{2}{3}} \int_{r_{\text{conv}}}^{r_{\text{int}}} z' \frac{X_1}{X_1(r_{\text{int}})} dr. \end{aligned} \quad (48)$$

The matching of the inhomogeneous solutions in the radiative and convective zones then gives

$$\begin{aligned} (\alpha_{\text{rad}} + \alpha_{\text{rad,p}}) \begin{pmatrix} S_+(0) \\ \partial_r S_+(0) \end{pmatrix} + (\beta_{\text{rad}} + \beta_{\text{rad,p}}) \begin{pmatrix} S_-(0) \\ \partial_r S_-(0) \end{pmatrix} \\ = (\alpha_{\text{conv}} + \alpha_{\text{conv,p}}) \begin{pmatrix} S_+(0) \\ \partial_r S_+(0) \end{pmatrix} + (\beta_{\text{conv}} + \beta_{\text{conv,p}}) \begin{pmatrix} S_-(0) \\ \partial_r S_-(0) \end{pmatrix}. \end{aligned} \quad (49)$$

Because the particular solution in the radiative zone vanishes at the interface, we obtain

$$\alpha_{\text{rad}} = \alpha_{\text{conv}} + \alpha_{\text{conv,p}}, \quad (50)$$

$$\beta_{\text{rad}} = \beta_{\text{conv}} + \beta_{\text{conv,p}}. \quad (51)$$

## 2.5.2. Matching WKBJ-Bessel

In the radiative zone, far from the interface, the functions  $J_{\frac{1}{3}}(\tau)$  and  $J_{-\frac{1}{3}}(\tau)$  for high values of  $\tau$  have the following asymptotic

form:  $J_{\pm\frac{1}{3}}(\tau) \sim \sqrt{\frac{2}{\pi\tau}} \cos\left(\tau \mp \frac{\pi}{6} - \frac{\pi}{4}\right)$ , which gives

$$\psi(\tau) = Z(\eta) + \frac{1}{\sqrt{\pi}} \left(\frac{2}{\tau}\right)^{\frac{1}{6}} \left[ \mathcal{A}_+ \cos\left(\tau - \frac{5\pi}{12}\right) + \mathcal{A}_- \cos\left(\tau - \frac{\pi}{12}\right) \right], \quad (52)$$

with

$$\begin{aligned} \mathcal{A}_+ &= \alpha_{\text{conv}} + \alpha_{\text{conv,p}} + \alpha_{\text{rad,p}}, \\ \mathcal{A}_- &= \beta_{\text{conv}} + \beta_{\text{conv,p}} + \beta_{\text{rad,p}}. \end{aligned} \quad (53)$$

When we define  $C = \frac{3^{\frac{1}{6}} v^{\frac{1}{3}}}{\sqrt{\pi}}$ , knowing that  $k_r = v\eta^{\frac{1}{2}}$  near the interface, we obtain

$$\psi(\tau) = Z(\eta) + \frac{C}{\sqrt{k_r}} \left[ \mathcal{A}_+ \cos\left(\tau - \frac{5\pi}{12}\right) + \mathcal{A}_- \cos\left(\tau - \frac{\pi}{12}\right) \right]. \quad (54)$$

Furthermore, we can note that  $\int_r^{r_{\text{int}}} k_r dr = \epsilon\tau$ . By introducing the constant  $\varphi = \tau + \tau_W - \tau_0 = \epsilon \int_{r_{\text{rad}}}^{r_{\text{int}}} k_r dr - \tau_0$ , the asymptotic solution becomes

$$\begin{aligned} \psi(\eta) &= Z(\eta) \\ &+ \frac{C}{\sqrt{k_r}} \left[ \mathcal{A}_+ \cos\left(\varphi - \frac{5\pi}{12}\right) + \mathcal{A}_- \cos\left(\varphi - \frac{\pi}{12}\right) \right] \cos(\tau_W - \tau_0) \\ &+ \frac{C}{\sqrt{k_r}} \left[ \mathcal{A}_+ \sin\left(\varphi - \frac{5\pi}{12}\right) + \mathcal{A}_- \sin\left(\varphi - \frac{\pi}{12}\right) \right] \sin(\tau_W - \tau_0). \end{aligned} \quad (55)$$

The matching with the WKBJ solution  $\psi = Z + C_W \frac{1}{\sqrt{k_r}} e^{i(\tau_W - \tau_0)}$  then leads to the following system:

$$\begin{cases} \mathcal{A}_+ \cos\left(\varphi - \frac{5\pi}{12}\right) + \mathcal{A}_- \cos\left(\varphi - \frac{\pi}{12}\right) = \frac{C_W}{C} \\ \mathcal{A}_+ \sin\left(\varphi - \frac{5\pi}{12}\right) + \mathcal{A}_- \sin\left(\varphi - \frac{\pi}{12}\right) = \epsilon i \frac{C_W}{C}, \end{cases} \quad (56)$$

which leads to (Ivanov et al. 2013)

$$\begin{cases} \alpha_{\text{conv}} + \alpha_{\text{conv,p}} + \alpha_{\text{rad,p}} = \frac{C_W}{C} \frac{\sin\left(\varphi - \frac{\pi}{12}\right) - \epsilon i \cos\left(\varphi - \frac{\pi}{12}\right)}{\sin\left(\frac{\pi}{3}\right)} \\ \beta_{\text{conv}} + \beta_{\text{conv,p}} + \beta_{\text{rad,p}} = -\frac{C_W}{C} \frac{\sin\left(\varphi - \frac{5\pi}{12}\right) - \epsilon i \cos\left(\varphi - \frac{5\pi}{12}\right)}{\sin\left(\frac{\pi}{3}\right)}. \end{cases} \quad (57)$$

Therefore we can express the WKBJ amplitude  $C_W$  as a function of the particular solution coefficients as follows:

$$\frac{\alpha_{\text{conv}}}{\beta_{\text{conv}}} (\beta_{\text{conv,p}} + \beta_{\text{rad,p}}) - \alpha_{\text{conv,p}} - \alpha_{\text{rad,p}} = \frac{-2C_W}{\sqrt{3}C} e^{i(\varphi - \frac{\pi}{12} - \frac{\pi}{2})}, \quad (58)$$

where we used the fact that  $\alpha_{\text{conv}} \ll \beta_{\text{conv}}$ . We finally obtain the following expression for  $C_W$  (Zahn 1975):

$$C_W = -K_0 e^{-i(\varphi - \frac{\pi}{12} - \frac{\pi}{2})}, \quad (59)$$

$$\text{with } K_0 = \frac{\sqrt{3}}{2} C \left[ \frac{\alpha_{\text{conv}}}{\beta_{\text{conv}}} (\beta_{\text{conv,p}} + \beta_{\text{rad,p}}) - \alpha_{\text{conv,p}} - \alpha_{\text{rad,p}} \right].$$

### 2.5.3. Closure of the system

In the previous sections, we were able to characterize the particular solutions in the convective and the radiative zone thanks to the following coefficients:

$$\begin{cases} \alpha_{\text{rad,p}} = -\frac{dZ}{d\eta}(0) \left(\frac{\nu}{3}\right)^{-\frac{2}{3}} \Gamma_1 \left(\frac{4}{3}\right) \\ \beta_{\text{rad,p}} = -Z(0) \Gamma \left(\frac{2}{3}\right) \\ \alpha_{\text{conv,p}} = -\alpha_1 \int_{r_{\text{conv}}}^{r_{\text{int}}} \Lambda^{-1} \rho_0 z' X_2 dr \\ \quad - \epsilon \rho_0^{\frac{1}{2}}(r_{\text{int}}) r_{\text{int}}^2 \Gamma \left(\frac{4}{3}\right) \left(\frac{\nu}{3}\right)^{-\frac{2}{3}} r_{\text{int}}^{-2} \int_{r_{\text{conv}}}^{r_{\text{int}}} z' \frac{X_1}{X_1(r_{\text{int}})} dr \\ \beta_{\text{conv,p}} = -\beta_1 \int_{r_{\text{conv}}}^{r_{\text{int}}} \Lambda^{-1} \rho_0 z' X_2 dr. \end{cases} \quad (60)$$

Then we can compute the quantity  $K_0$  as follows:

$$\begin{aligned} K_0 = \mathcal{T}_0 + \frac{3\Gamma\left(\frac{4}{3}\right)}{2\sqrt{\pi}} \left(\frac{\nu}{3}\right)^{-\frac{1}{3}} \rho_0^{\frac{1}{2}}(r_{\text{int}}) r_{\text{int}}^2 \\ \times \left\{ \left[ -\epsilon \frac{d(\rho_0^{-\frac{1}{2}} X_h)_{\text{int}}}{dr} - \frac{dZ(0)}{d\eta} \right] \left( \frac{\varphi_T}{g_0} \right)_{\text{int}} + \epsilon r_{\text{int}}^{-2} \int_{r_{\text{conv}}}^{r_{\text{int}}} z' \frac{X_1}{X_1(r_{\text{int}})} dr \right\} \end{aligned} \quad (61)$$

where

$$\mathcal{T}_0 = -\frac{\sqrt{3}}{2} C \left( \frac{\alpha_{\text{conv}}}{\beta_{\text{conv}}} \beta_1 - \alpha_1 \right) \int_{r_{\text{conv}}}^{r_{\text{int}}} \Lambda^{-1} \rho_0 z' X_2 dr. \quad (62)$$

Furthermore, from Eq. (38) we have

$$\begin{aligned} r_{\text{int}}^{-2} \int_{r_{\text{conv}}}^{r_{\text{int}}} z' \frac{X_1}{X_1(r_{\text{int}})} dr = r_{\text{int}}^{-2} \mathcal{F}_1 + \mathcal{T}_1 \\ + \left( \frac{\varphi_T}{g_0} \right)_{\text{int}} \left\{ -\frac{\rho_0'(r_{\text{int}})}{\rho_0(r_{\text{int}})} - \frac{(\rho_0^{-\frac{1}{2}} Z)'_{\text{int}}}{(\rho_0^{-\frac{1}{2}} Z)_{\text{int}}} + \frac{X_1'(r_{\text{int}})}{X_1(r_{\text{int}})} \right\}, \end{aligned} \quad (63)$$

where

$$\begin{aligned} \mathcal{F}_1 = \int_{r_{\text{conv}}}^{r_{\text{int}}} \left[ \left( \frac{r^2 \varphi_T}{g_0} \right)'' - \frac{l(l+1)}{r^2} \left( \frac{r^2 \varphi_T}{g_0} \right) \right] \frac{X_1}{X_1(r_{\text{int}})} dr, \\ \mathcal{T}_1 = \left( \frac{\varphi_T}{g_0} \right)_{r_{\text{conv}}} \left( \frac{r_{\text{conv}}}{r_{\text{int}}} \right)^2 \\ \times \left\{ \frac{\rho_0'(r_{\text{conv}})}{\rho_0(r_{\text{conv}})} + \frac{(\rho_0^{-\frac{1}{2}} Z)'_{r_{\text{conv}}}}{(\rho_0^{-\frac{1}{2}} Z)_{r_{\text{conv}}}} \left[ \frac{X_1(r_{\text{conv}})}{X_1(r_{\text{int}})} - \frac{X_1'(r_{\text{conv}})}{X_1(r_{\text{int}})} \right] \right\}, \end{aligned} \quad (64)$$

From this, we obtain

$$K_0 = \mathcal{T}_0 + \frac{3\Gamma\left(\frac{4}{3}\right)}{2\sqrt{\pi}} \left(\frac{\nu}{3}\right)^{-\frac{1}{3}} \rho_0^{\frac{1}{2}}(r_{\text{int}}) r_{\text{int}}^2 \left\{ \epsilon r_{\text{int}}^{-2} \mathcal{F}_1 + \epsilon \mathcal{T}_1 + \mathcal{T}_2 \right\}, \quad (65)$$

with

$$\mathcal{T}_2 = \left( \frac{\varphi_T}{g} \right)_{r_{\text{int}}} \left(\frac{\nu}{3}\right)^{\frac{2}{3}} \frac{\Gamma\left(\frac{2}{3}\right)}{\Gamma\left(\frac{4}{3}\right)} \frac{C_2}{\beta_1 C_1}. \quad (66)$$

The constants of integration  $C_1$  and  $C_2$ , defined in Eq. (36), correspond to the homogeneous solutions in the convective zone. In this way, we are able to assess the WKB amplitude of the tidal gravity waves from stellar properties and the tidal potential. This quantity is of prime importance for estimating the energy and angular momentum fluxes carried by tidal internal gravity waves.

## 3. Tidal dissipation in stellar radiative zones

### 3.1. Energy flux and luminosity

We return to the perturbed equations of hydrodynamics, assuming the Cowling approximation (Cowling 1941),

$$\begin{cases} \partial_t \rho_1 + \mathbf{v}_1 \cdot \nabla \rho_0 + \rho_0 \nabla \cdot \mathbf{v}_1 = 0 \\ \partial_t \mathbf{v}_1 = -\frac{1}{\rho_0} \nabla p_1 + \frac{\rho_1}{\rho_0^2} \nabla p_0 - \nabla U_T \\ \frac{1}{\rho_0} [\partial_t p_1 + (\mathbf{v}_1 \cdot \nabla) p_0] - \frac{\Gamma_1}{\rho_0} [\partial_t \rho_1 + (\mathbf{v}_1 \cdot \nabla) \rho_0] = 0. \end{cases} \quad (67)$$

We introduce the buoyancy term  $\mathbf{b} = \frac{\rho_1}{\rho_0^2} \nabla p_0 = -\frac{g_0 \rho_1}{\rho_0} \mathbf{e}_r$ , which verifies in the anelastic approximation

$$\partial_t \mathbf{b} = -N^2 \mathbf{v}_1 \cdot \mathbf{e}_r. \quad (68)$$

The momentum equation then gives

$$\partial_t \mathbf{v}_1 \cdot \mathbf{v}_1 = -\frac{1}{\rho_0} \nabla p_1 \cdot \mathbf{v}_1 + \mathbf{b} \cdot \mathbf{v}_1 - \nabla U_T \cdot \mathbf{v}_1, \quad (69)$$

which leads to

$$\partial_t \left[ \frac{1}{2} \rho_0 v_1^2 + \rho_0 \frac{b^2}{2N^2} \right] + \nabla \cdot [(p_1 + \rho_0 U_T) \mathbf{v}_1] = p_1 \nabla \cdot \mathbf{v}_1 - U_T \partial_t \rho_1. \quad (70)$$

From the anelastic approximation, we can simplify the continuity equation because  $\partial_t \rho_1$  can be neglected. Furthermore, the anelastic approximation reduces to the Boussinesq approximation at low frequencies, which means that we can assume that  $\nabla \cdot \mathbf{v}_1 = 0$ . In this framework, the conservation of energy can be expressed as follows:

$$\partial_t e + \nabla \cdot \mathbf{F}_E = 0, \quad (71)$$

where  $e = \frac{1}{2} \rho_0 v_1^2 + \rho_0 \frac{b^2}{2N^2}$  is the energy density of the fluid, the sum of the kinetic energy density  $1/2 \rho_0 v_1^2$  and of the potential energy density  $\rho_0 b^2 / 2N^2$ , and  $\mathbf{F}_E = (p_1 + \rho_0 U_T) \mathbf{v}_1$  is the energy flux carried by the tidal internal gravity waves.

When we decompose the relevant quantities of the spherical harmonics, the temporal mean of the energy flux along the direction of propagation becomes

$$\begin{aligned} F_E(r, \theta, \varphi) &= \frac{1}{2} \Re \{ \rho_0(r) [y(r) + \varphi_T(r)] (-i\omega \xi_r(r))^* \} |Y_l^m(\theta, \varphi)|^2 \\ &= -\frac{\rho_0 \omega}{2} \Im \{ \chi(r) \xi_r^*(r) \} |Y_l^m(\theta, \varphi)|^2. \end{aligned} \quad (72)$$

To assess the energy flux carried by a gravity wave traveling in the radiative zone far from the interface, we consider only the radial displacement associated with the dynamical tide in its WKB form,  $\xi_r = C_W \rho_0^{-\frac{1}{2}} r^{-2} k_r^{-\frac{1}{2}} \exp[\epsilon i(\tau_W - \tau_0)]$ . Furthermore, when we use the anelastic approximation on Eqs. (12), we obtain

$$\chi = \frac{\omega^2}{l(l+1)} \partial_r (r^2 \xi_r). \quad (73)$$

The mean energy flux carried by the waves then becomes

$$F_E = -\epsilon \frac{\omega^3}{2l(l+1)} |C_W|^2 r^{-2} |Y_l^m|^2. \quad (74)$$

From this expression, we can compute the energy luminosity

$$L_E(r) = \int_0^{2\pi} \int_0^\pi F_E(r, \theta, \varphi) r^2 \sin \theta \, d\theta d\varphi \text{ as}$$

$$L_E = -\epsilon \frac{1}{2} \frac{\omega^3}{l(l+1)} |C_W|^2, \quad (75)$$

where the constant  $C_W$  can be computed through the expression of  $K_0$  in Eq. (65). As expected from adiabatic oscillations, the energy luminosity is conserved. Furthermore, in the case of an inward energy transport (for which  $\epsilon = 1$ ; see Table 1), the energy luminosity is negative, while in the case of an outward energy transport (for which  $\epsilon = -1$ ; see Table 1),  $L_E$  is positive.

### 3.2. Computation of the tidal torque

In the radiative zone, far from the interface, we can express the azimuthal displacement from the radial displacement in its WKBJ form as

$$\begin{aligned} \xi_h &= \frac{X}{\omega^2 r} \\ &= \epsilon i \frac{r k_r}{l(l+1)} \xi_r. \end{aligned} \quad (76)$$

This expression then leads to the azimuthal velocity (Zahn et al. 1997)

$$v_{1\varphi} = -\epsilon m \frac{r k_r}{l(l+1)} \frac{v_{1r}}{\sin \theta}. \quad (77)$$

From those calculations, we can compute the temporal mean of angular momentum flux along the direction of propagation as

$$\begin{aligned} F_J(r, \theta, \varphi) &= \frac{1}{2} \rho_0 r \sin \theta \Re \left\{ v_{1\varphi}(r, \theta, \varphi) v_{1r}^*(r, \theta, \varphi) \right\} \\ &= \frac{m}{\omega} F_E(r, \theta, \varphi). \end{aligned} \quad (78)$$

From this expression, we can compute the mean luminosity of angular momentum  $L_J(r) = \int_0^{2\pi} \int_0^\pi F_J(r, \theta, \varphi) r^2 \sin \theta \, d\theta d\varphi$ :

$$L_J = -\epsilon \frac{m}{2} \frac{\omega^2}{l(l+1)} |C_W|^2, \quad (79)$$

which represents the angular momentum transported by tidal gravity waves per unit of time. This quantity is also conserved as we consider adiabatic oscillations. Furthermore, we find that prograde waves ( $m > 0$ ) transport angular momentum toward the center of the star in the case of an inward energy transport ( $\epsilon = 1$ , corresponding to the configuration of solar-type stars), while they deposit angular momentum near the stellar surface in the case of an outward energy transport ( $\epsilon = -1$ , corresponding to the configuration of massive and intermediate-mass stars). Because we assume that tidal gravity waves are entirely dissipated in the radiative zone before any reflection (see Sect. 2.1), the star then undergoes a tidal torque  $T$  coming from the deposition of angular momentum by the excited waves. This means that prograde waves transporting energy inward in the solar-type configuration and outward in the massive-star configuration both lead to a spin-up of the radiative zone (we refer to Appendix E for a detailed computation), which leads to

$$T = -\epsilon L_J. \quad (80)$$

Inserting Eq. (79) into Eq. (80) leads to

$$T = \frac{m}{2} \frac{\omega^2}{l(l+1)} |C_W|^2, \quad (81)$$

which is independent of the direction of propagation of the waves. This expression has to be compared to the following formulation in the case of a coplanar and circular system (Murray & Dermott 1999),

$$|T| = \frac{9}{4Q'} \frac{m_p^2}{M_\star} R_\star^2 \frac{n^4}{\omega_{\text{dyn}}^2}, \quad (82)$$

where  $M_\star$  is the stellar mass,  $R_\star$  is the stellar radius,  $m_p$  is the planet mass,  $n$  is the mean motion,  $\omega_{\text{dyn}}^2 = \frac{GM_\star}{R_\star^3}$ , and  $Q'$  is a modified quality factor, defined as the ratio of the total energy stored in the tidal velocity field divided by the energy dissipated over one planetary revolution (Goldreich 1963; Kaula 1964; MacDonald 1964). This quantity can be linked to the Love number  $k_2$ , which is the ratio of the perturbed gravitational potential of the star divided by the tidal potential at the stellar surface, as

$$Q' = \frac{3}{2|\mathfrak{I}(k_2)|}. \quad (83)$$

From this formulation, we can assess the tidal dissipation and the modified quality factor as

$$|\mathfrak{I}(k_2)| = \frac{1}{3} \frac{|m|}{l(l+1)} \frac{M_\star}{m_p^2 R_\star^2} \frac{\omega_{\text{dyn}}^2 \omega^2}{n^4} |C_W|^2, \quad (84)$$

$$Q' = \frac{9}{2} \frac{l(l+1)}{|m|} \frac{m_p^2 R_\star^2}{M_\star} \frac{n^4}{\omega_{\text{dyn}}^2 \omega^2} \frac{1}{|C_W|^2}. \quad (85)$$

## 4. Application to stellar structures

### 4.1. Dynamical tide in intermediate-mass and massive stars: the Zahn (1975) prescription

In the case of a massive star, we consider a bilayer structure with a convective core and a radiative envelope. The energy transported by a tidal gravity wave therefore propagates outward, toward the stellar surface. This gives in our formulation  $r_{\text{conv}} = 0$ ,  $r_{\text{rad}} = R_\star$  and  $\epsilon = -1$ , as already presented in Table 1. Furthermore, we assume that the radial displacement and the tidal potential vanish at the center due to spherical symmetry. Because Eq. (12) in the anelastic approximation leads to

$$\partial_r (r^2 \xi_r) + \frac{\partial_r p_0}{\Gamma_1 p_0} (r^2 \xi_r) = \frac{l(l+1)}{\omega^2} \varphi_T, \quad (86)$$

the conditions at the center of the star can be reduced to

$$\xi_r(0) = 0, \quad (87)$$

$$\partial_r \xi_r(0) = 0. \quad (88)$$

Furthermore, as we consider a convective core, we translate the aforementioned conditions by means of the function  $X = \rho_0 r^2 \xi_r$ . We then obtain  $X(0) = X'(0) = 0$ . When we assume that  $X_1$  is the solution regular at the center, then  $C_2 = 0$ , that is,  $\mathcal{T}_0 = \mathcal{T}_2 = 0$ . To

keep a nonzero solution, we therefore need to impose  $X_1(0) = 0$ . Because  $r_{\text{conv}} = 0$ , we also have  $\mathcal{T}_1 = 0$ . In this way, we can now express  $K_0$  as

$$K_0 = -\frac{3\Gamma\left(\frac{4}{3}\right)}{2\sqrt{\pi}} \left(\frac{v}{3}\right)^{-\frac{1}{3}} \rho_0^{\frac{1}{2}}(r_{\text{int}}) \mathcal{F}, \quad (89)$$

where

$$\mathcal{F} = \int_0^{r_{\text{int}}} \left[ \left( \frac{r^2 \varphi_T}{g_0} \right)'' - \frac{l(l+1)}{r^2} \left( \frac{r^2 \varphi_T}{g_0} \right) \right] \frac{X_1}{X_1(r_{\text{int}})} dr \quad (90)$$

can easily be linked to the  $H_l$  parameter introduced by Zahn (1970, 1975). To compare with the results of Zahn (1975), we proceeded as follows. From the expression of  $v$  in Eq. (24), we have

$$\begin{aligned} K_0 &= -\left(\frac{l(l+1)}{\omega^2}\right)^{\frac{1}{4}} \frac{\sqrt{3}\Gamma\left(\frac{4}{3}\right)}{2\sqrt{\pi}} \left(\frac{v}{3}\right)^{-\frac{5}{6}} \rho_0^{\frac{1}{2}}(r_{\text{int}}) \left(\frac{1}{r_{\text{int}}^2} \left| \frac{dN^2}{dr} \right|_{\text{int}}\right)^{\frac{1}{4}} \mathcal{F} \\ &= -\left(\frac{l(l+1)}{\omega^2}\right)^{\frac{1}{4}} K_{0,Z75}, \end{aligned} \quad (91)$$

where  $K_{0,Z75}$  is the amplitude of the WKBJ solution as derived in Zahn (1975). Furthermore, in the present paper, the WKBJ solution is written as  $\xi_r = -\frac{\varphi_T}{g_0} + C_W \rho_0^{-\frac{1}{2}} r^{-2} \frac{1}{\sqrt{k_r}} e^{-i(\tau_W - \tau_0)}$ , while in Zahn (1975), the following formulation was used:

$$\xi_r = -\frac{\varphi_T}{g_0} - C_{Z75} \rho_0^{-\frac{1}{2}} r^{-2} \left(\frac{N^2}{r^2}\right)^{-\frac{1}{4}} e^{-i(\tau_W - \tau_0)}. \quad (92)$$

In order to keep consistent formulations, we therefore have

$$C_W = -\left(\frac{l(l+1)}{\omega^2}\right)^{\frac{1}{4}} C_{Z75}. \quad (93)$$

This change of convention then explains the different expressions obtained for the  $K_0$  term. From Eq. (75) the energy luminosity then becomes

$$L_E = \frac{1}{2} \frac{\omega^2}{\sqrt{l(l+1)}} K_{0,Z75}^2, \quad (94)$$

which is identical to the expression derived by Zahn (1975). From the expression of  $K_0$ , the energy luminosity becomes

$$L_E = -\frac{3^{\frac{2}{3}} \Gamma^2\left(\frac{1}{3}\right)}{8\pi} \omega^{\frac{11}{3}} [l(l+1)]^{-\frac{4}{3}} \rho_0(r_{\text{int}}) r_{\text{int}} \left| \frac{dN^2}{d \ln r} \right|_{r_{\text{int}}}^{-\frac{1}{3}} \mathcal{F}^2, \quad (95)$$

which is similar to the Goodman & Dickson (1998) formulation in the case of low-mass stars. The tidal torque and the corresponding tidal dissipation can then be computed as follows:

$$|T| = \frac{|m|}{\omega} \frac{3^{\frac{2}{3}} \Gamma^2\left(\frac{1}{3}\right)}{8\pi} \omega^{\frac{11}{3}} [l(l+1)]^{-\frac{4}{3}} \rho_0(r_{\text{int}}) r_{\text{int}} \left| \frac{dN^2}{d \ln r} \right|_{r_{\text{int}}}^{-\frac{1}{3}} \mathcal{F}^2, \quad (96)$$

$$\begin{aligned} |\mathfrak{J}(k_2)| &= \frac{3^{-\frac{1}{3}} \Gamma^2\left(\frac{1}{3}\right)}{4\pi} |m| [l(l+1)]^{-\frac{4}{3}} \\ &\times \frac{\omega^{\frac{8}{3}} G M_\star^2}{n^4 m_p^2 R_\star^5} \rho_0(r_{\text{int}}) r_{\text{int}} \left| \frac{dN^2}{d \ln r} \right|_{r_{\text{int}}}^{-\frac{1}{3}} \mathcal{F}^2. \end{aligned} \quad (97)$$

## 4.2. Dynamical tide in low-mass stars

We now aim to estimate the tidal dissipation in the radiative zone of solar-type stars. After a general calculation of the associated tidal torque, we propose alternative formulations of the same quantity, especially in the case of a star with a thin convective layer. Finally, we apply our formalism to a trilayer structure.

### 4.2.1. General computation of the tidal dissipation

In the case of a solar-type star, we consider a bilayer structure with a radiative core and a convective envelope. The energy transported by the wave therefore propagates inward, toward the center. This gives in our formulation (see Table 1)  $r_{\text{conv}} = R_\star$ ,  $r_{\text{rad}} = 0$ , and  $\epsilon = 1$ . We assume that the density at the stellar surface vanishes. This hypothesis is valid for a polytropic model and allows us to automatically fulfill a stress-free boundary condition, according to which the Lagrangian pressure perturbation vanishes. Considering the same surface condition for a no-zero density affects our results only marginally. A photospheric density slightly modifies the conditions of excitation of tidal gravity waves (for more details, we refer to Appendix C). Boundary conditions at the stellar surface will be extensively investigated in a future work. For a zero density at the stellar surface, we obtain

$$X(R_\star) = \rho_0(R_\star) R_\star^2 \xi_r(R_\star) = 0. \quad (98)$$

Furthermore, we choose a basis solution in the convective zone  $X_1$  such as  $X_1(R_\star) = 0$ . Because  $X(R_\star) = C_1 X_1(R_\star) + C_2 X_2(R_\star)$ , we then need  $C_2 = 0$  to fulfill the condition at the stellar surface, which leads to  $\mathcal{T}_0 = \mathcal{T}_2 = 0$ . Furthermore, when we consider stellar matter as a polytrope near the stellar surface, we can define  $\theta, K, n$  as

$$P_0 = K \rho_0^{1+\frac{1}{n}}, \quad (99)$$

$$\rho_0 = \rho_c \theta^n, \quad (100)$$

where  $\rho_c$  is the density at the center (Chandrasekhar 1939; Kippenhahn & Weigert 1994). By defining a dimensionless radius  $\xi$ , the stellar mass and the stellar radius can be defined from the solutions of the Lane-Emden equation as

$$R_\star = \left[ \frac{(n+1) K \rho_c^{\frac{1}{n}-1}}{4\pi G} \right]^{\frac{1}{2}} \xi_1, \quad (101)$$

$$M_\star = -4\pi \left[ \frac{(n+1) K \rho_c^{\frac{1}{n}-1}}{4\pi G} \right]^{\frac{3}{2}} \rho_c^{\frac{3-n}{2n}} \xi_1^2 \left( \frac{d\theta}{d\xi} \right)_{\xi_1}, \quad (102)$$

where  $\xi_1$  is the first zero of  $\theta(\xi)$ . Because the mass and radius take finite values, we obtain

$$\frac{\rho'_0}{\rho_0} = \frac{n}{\theta} \frac{d\theta}{d\xi} \xrightarrow{r \rightarrow R_\star} -\infty. \quad (103)$$

Near the surface,  $X_1$  therefore is a solution of the following equation:

$$X'' - \frac{\rho'_0}{\rho_0} X' = 0, \quad (104)$$

which leads to  $X'_1 \propto \rho_0$ . Therefore we obtain  $X'_1(R_\star) = 0$ . From these considerations, we now have  $\mathcal{T}_1 = 0$  and

$$K_0 = -\frac{3\Gamma\left(\frac{4}{3}\right)}{2\sqrt{\pi}}\left(\frac{v}{3}\right)^{-\frac{1}{3}}\rho_0^{\frac{1}{2}}(r_{\text{int}})\mathcal{F}, \quad (105)$$

with

$$\mathcal{F} = \int_{r_{\text{int}}}^{R_\star} \left[ \left( \frac{r^2 \varphi_T}{g_0} \right)'' - \frac{l(l+1)}{r^2} \left( \frac{r^2 \varphi_T}{g_0} \right) \right] \frac{X_1}{X_1(r_{\text{int}})} dr. \quad (106)$$

The energy luminosity then becomes

$$L_E = -\frac{3^{\frac{3}{2}}\Gamma^2\left(\frac{1}{3}\right)}{8\pi}\omega^{\frac{11}{3}}[l(l+1)]^{-\frac{4}{3}}\rho_0(r_{\text{int}})r_{\text{int}}\left|\frac{dN^2}{d\ln r}\right|_{r_{\text{int}}}^{-\frac{1}{3}}\mathcal{F}^2. \quad (107)$$

This expression is equivalent to the [Goodman & Dickson \(1998\)](#) prescription if

$$\left|\partial_r \xi_r^{\text{dyn}}\right|_{r_{\text{int}}} = r_{\text{int}}^{-2}\mathcal{F}, \quad (108)$$

where  $\xi_r^{\text{dyn}}$  is the radial displacement linked to the dynamical tide. We can ensure that this condition is fulfilled from straightforward calculations by expressing the radial displacement  $\xi_r$  in the  $(S_+, S_-)$  basis, knowing that  $C_2 = \mathcal{T}_1 = 0$  (we refer to [Appendix B](#) for more details). The tidal torque  $T$  can be computed as

$$|T| = \frac{|m|}{\omega} \frac{3^{\frac{3}{2}}\Gamma^2\left(\frac{1}{3}\right)}{8\pi}\omega^{\frac{11}{3}}[l(l+1)]^{-\frac{4}{3}}\rho_0(r_{\text{int}})r_{\text{int}}\left|\frac{dN^2}{d\ln r}\right|_{r_{\text{int}}}^{-\frac{1}{3}}\mathcal{F}^2. \quad (109)$$

By comparing this expression to the [Murray & Dermott \(1999\)](#) formulation in Eq. (82), we can assess the tidal dissipation as

$$|\mathfrak{J}(k_2)| = \frac{3^{-\frac{1}{3}}\Gamma^2\left(\frac{1}{3}\right)}{4\pi}|m|[l(l+1)]^{-\frac{4}{3}} \times \frac{\omega^{\frac{8}{3}}GM_\star^2}{n^4 m_p^2 R_\star^5} \rho_0(r_{\text{int}})r_{\text{int}}\left|\frac{dN^2}{d\ln r}\right|_{r_{\text{int}}}^{-\frac{1}{3}}\mathcal{F}^2. \quad (110)$$

#### 4.2.2. Alternative formulation of the forcing term

We now aim to simplify the forcing term  $\mathcal{F}$  in the case of a solar-type star to better understand this contribution to tidal dissipation. The behavior of the tidal potential is ruled by the Poisson equation,

$$\partial_r(r^2 \partial_r \varphi_T) = l(l+1)\varphi_T. \quad (111)$$

The gravitational acceleration can be computed from the mean density  $\bar{\rho}$  inside a sphere of radius  $r$  through Gauss's law

$$g_0 = \frac{4}{3}\pi G \bar{\rho} r, \quad (112)$$

with  $\bar{\rho} = \frac{3}{4\pi r^3} \int_0^r 4\pi r_1^2 \rho(r_1) dr_1$ . From these expressions, we obtain

$$\begin{cases} \partial_r \bar{\rho} = \frac{3}{r}(\rho(r) - \bar{\rho}) \\ \partial_r g_0 = \frac{g}{r} + 4\pi G(\rho(r) - \bar{\rho}). \end{cases} \quad (113)$$

When we define  $Y = \frac{r^2 \varphi_T}{g_0}$ , we have

$$Y' = \left[ 1 + 3 \left( 1 - \frac{\rho}{\bar{\rho}} \right) \right] \frac{Y}{r} + \frac{r^2 \varphi_T}{g_0}, \quad (114)$$

which by assuming slow variations of the stellar density, leads to ([Zahn 1970, 1975](#))

$$Y'' - 6 \left( 1 - \frac{\rho}{\bar{\rho}} \right) \frac{Y'}{r} - \left[ l(l+1) - 12 \left( 1 - \frac{\rho}{\bar{\rho}} \right) \right] \frac{Y}{r^2} = 0. \quad (115)$$

The forcing term  $\mathcal{F}$  therefore becomes ([Kushnir et al. 2017](#))

$$\mathcal{F} = \int_{r_{\text{int}}}^{R_\star} 6 \left( 1 - \frac{\rho}{\bar{\rho}} \right) \left[ \frac{1}{r} \left( \frac{r^2 \varphi_T}{g_0} \right)' - \frac{2}{r^2} \left( \frac{r^2 \varphi_T}{g_0} \right) \right] \frac{X_1}{X_1(r_{\text{int}})} dr \quad (116)$$

#### 4.2.3. Case of a simplified bilayer structure for a solar-type star

We assume a bilayer structure for a given solar-type star in this section for which both the radiative core and the convective envelope are assumed to be homogeneous, with respective constant densities  $\rho_r$  and  $\rho_c \ll \rho_r$ . We also assume that the depth of the convective layer is smaller than the stellar radius. We introduce the aspect ratios

$$\alpha = \frac{R_r}{R_\star}, \quad (117)$$

$$\beta = \frac{M_r}{M_\star}, \quad (118)$$

$$\gamma = \frac{\rho_c}{\rho_r} = \frac{\alpha^3(1-\beta)}{\beta(1-\alpha^3)}, \quad (119)$$

where  $R_r$  is the radius of the radiative zone and  $M_r$  is its mass. With this configuration, we have

$$\bar{\rho} \approx \rho_r = \frac{3M_\star}{4\pi R_\star^3} \frac{\beta}{\alpha^3}, \quad (120)$$

$$g_0 = \frac{\beta}{\alpha^3} \omega_{\text{dyn}}^2 r, \quad (121)$$

with  $\omega_{\text{dyn}}^2 = \frac{GM_\star}{R_\star^3}$ . The forcing term  $\mathcal{F}$  in its alternative form can therefore be expressed as

$$\mathcal{F} = 6(1-\gamma) \int_{r_{\text{int}}}^{R_\star} \left[ \frac{1}{r} \left( \frac{r^2 \varphi_T}{g_0} \right)' - \frac{2}{r^2} \left( \frac{r^2 \varphi_T}{g_0} \right) \right] \frac{X_1}{X_1(r_{\text{int}})} dr. \quad (122)$$

Furthermore, in the case of a solar-type star, we showed that

$$X'_1(r) \propto \rho_0(r), \text{ with } 1 - \frac{r}{R_\star} \ll 1. \quad (123)$$

From this we obtain

$$\frac{X_1(r)}{X_1(r_{\text{int}})} = \frac{\rho_c(R_\star - r)}{\rho_c(R_\star - r_{\text{int}})} = \frac{1}{1 - \alpha} \left(1 - \frac{r}{R_\star}\right). \quad (124)$$

The forcing term then becomes

$$\mathcal{F} = 6 \frac{1 - \gamma}{1 - \alpha} \int_{r_{\text{int}}}^{R_\star} \left[ \frac{1}{r} \left( \frac{r^2 \varphi_T}{g} \right)' - \frac{2}{r^2} \left( \frac{r^2 \varphi_T}{g} \right) \right] \left(1 - \frac{r}{R_\star}\right) dr. \quad (125)$$

By introducing the quantity  $\Psi = \frac{\varphi_T}{r^2}$ , we can write  $Y = \frac{r^2 \varphi_T}{g}$  independent of the stellar radius as

$$Y = \frac{\alpha^3}{\beta} \frac{\Psi}{\omega_{\text{dyn}}^2} r^3. \quad (126)$$

From this we obtain

$$\mathcal{F} = 3 \frac{1 - \gamma}{1 - \alpha} \frac{\alpha^5}{\beta} \left( \frac{2\alpha}{3} - 1 \right) R_\star^2 \frac{\Psi}{\omega_{\text{dyn}}^2}. \quad (127)$$

By comparing with the [Goodman & Dickson \(1998\)](#) prescription, we obtain

$$\partial_r \xi_r^{\text{dyn}}(r_{\text{int}}) = 3 \frac{1 - \gamma}{1 - \alpha} \frac{\alpha^3}{\beta} \left( \frac{2\alpha}{3} - 1 \right) \frac{\Psi}{\omega_{\text{dyn}}^2}. \quad (128)$$

This prescription justifies the parametrizations of [Goodman & Dickson \(1998\)](#) and [Barker & Ogilvie \(2010\)](#) analytically. This leads to the following tidal dissipation:

$$\begin{aligned} \frac{3}{2Q'} &= \frac{3^{\frac{8}{3}} \Gamma^2 \left( \frac{1}{3} \right)}{16\pi^2} |m| [l(l+1)]^{-\frac{4}{3}} \\ &\times \frac{\omega^{\frac{8}{3}}}{n^4} \frac{M_\star R_\star^3}{G} \mathcal{E}(\alpha, \beta) \left| \frac{dN^2}{d \ln r} \right|_{r_{\text{int}}}^{-\frac{1}{3}} \frac{\Psi^2}{m_p^2}, \end{aligned} \quad (129)$$

where  $\mathcal{E}(\alpha, \beta) = \frac{\alpha^{11}(1-\beta)(1-\gamma)^2}{\beta^2(1-\alpha^3)(1-\alpha)^2} \left( \frac{2\alpha}{3} - 1 \right)^2$ . When we consider the amplitude of the largest tide for a coplanar and circular orbit ([Ogilvie & Lin 2004](#); [Barker & Ogilvie 2010](#)),

$$\Psi = \sqrt{\frac{6\pi}{5}} \frac{m_p}{M_\star} n^2, \quad (130)$$

we obtain a simplified expression for the tidal dissipation,

$$\frac{3}{2Q'} = \frac{3^{\frac{11}{3}} \Gamma^2 \left( \frac{1}{3} \right)}{40\pi} |m| [l(l+1)]^{-\frac{4}{3}} \omega^{\frac{8}{3}} \frac{R_\star^3}{GM_\star} \left| \frac{dN^2}{d \ln r} \right|_{r_{\text{int}}}^{-\frac{1}{3}} \mathcal{E}(\alpha, \beta). \quad (131)$$

#### 4.3. Tidal dissipation for a trilayer structure

In main-sequence F-type stars, a convective core is present in addition to the envelope ([Kippenhahn & Weigert 1994](#)). The dominating CNO cycle is extremely sensitive to the temperature and concentrates the energy production at low radii. In this configuration, convection therefore is the most efficient process in the central region to transport energy toward the center. A convective core also exists in evolved stars, for which the dissipation of  $g$ -modes is important ([Schlaufman & Winn 2013](#);

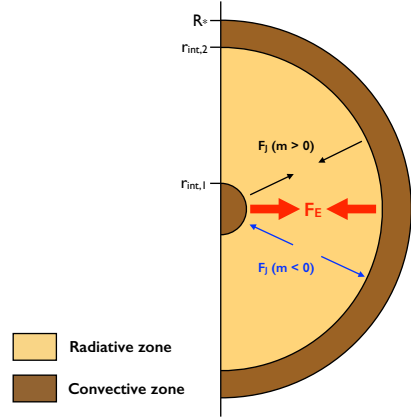


**Fig. 3.** Configurations of the radiative and convective spherical shells for the case of a trilayer structure. In brown we show the convective layer. In orange we plot the radiative layer. The red arrows represent the energy fluxes ( $F_E$ ), the black arrows correspond to the angular momentum fluxes ( $F_j$ ) for prograde waves ( $m > 0$ ), and the blue arrows stand for the angular momentum fluxes in the case of retrograde waves ( $m < 0$ ).

[Essick & Weinberg 2016](#); [Weinberg et al. 2017](#)). More complex stellar structures may therefore have to be investigated with our formalism.

As tidally excited modes are observed in this type of stars, for example, in heartbeat stars (we refer to [Fuller 2017](#) for an extensive study), the formation of standing  $g$ -modes is generally not prevented. For instance, following [Barker & Ogilvie \(2010\)](#), wave braking may occur in the central part of the star if the companion is massive enough (we refer to [Barker 2020](#) and Appendix D for a derivation of this criterion). However, this configuration is more likely to occur for stars older than 2 Gyr ([Barker 2020](#)), whose convective core has already disappeared. The only remaining possibility to prevent the formation of a standing mode is a potential interaction with a critical layer ([Alvan et al. 2013](#)). At the beginning of the MS, the rotation period of the stellar radiative zone can be comparable to the orbital period of the companion and can be short enough to ensure efficient tidal interaction (e.g., [Gallet & Bouvier 2015](#); [Amard et al. 2019](#)). We present the general formalism for this potential (rare) event. In any case, our prescription may no longer provide an upper bound of tidal dissipation for this type of stars. Tidal gravity modes may be resonantly excited and can produce more dissipation than progressive waves.

As shown in Fig. 3, we consider a trilayer structure with a convective core delimited by the interface located at  $r = r_{\text{int},1}$ , an intermediate radiative layer, and a convective envelope between  $r = r_{\text{int},2}$  and  $r = R_\star$ . Inside the radiative zone, the tidal gravity wave therefore propagates inward and outward from the interfaces. We assume that all the energy carried by a gravity wave from an interface is dissipated in the radiative zone before reaching the other interface. In this way, the outward and inward gravity waves are decoupled. The corresponding values of  $r_{\text{int}}$ ,  $r_{\text{rad}}$ ,  $r_{\text{conv}}$ , and  $\epsilon$  in the case of an outward and inward energy transport are presented in Table 2.

Far from the interfaces in the radiative zone, the radial displacement of the inward and outward gravity waves can be written in the following WKBJ form:

$$\xi_{r,\text{in}} = C_{W,\text{in}} \rho_0^{-\frac{1}{2}} r^{-2} k_r^{-\frac{1}{2}} \exp[i(\tau_W - \tau_0)], \quad (132)$$

$$\xi_{r,\text{out}} = C_{W,\text{out}} \rho_0^{-\frac{1}{2}} r^{-2} k_r^{-\frac{1}{2}} \exp[-i(\tau_W - \tau_0)]. \quad (133)$$

**Table 2.** Values of  $r_{\text{int}}$ ,  $r_{\text{rad}}$ ,  $r_{\text{conv}}$ , and  $\epsilon$  in the case of a trilayer structure.

Configuration	$r_{\text{int}}$	$r_{\text{rad}}$	$r_{\text{conv}}$	$\epsilon$
Inward energy transport	$r_{\text{int},2}$	$r_{\text{int},1}$	$R_\star$	1
Outward energy transport	$r_{\text{int},1}$	$r_{\text{int},2}$	0	-1

Each contribution transports angular momentum within the radiative zone, quantified by the corresponding luminosity,

$$L_{J,\text{in/out}} = -\epsilon \frac{m}{2} \frac{\omega^2}{l(l+1)} |C_{W,\text{in/out}}|^2. \quad (134)$$

As we consider the net torque applied on the radiative zone as a whole, we only focus on the transport of angular momentum at the convective-radiative interfaces (we refer to Appendix E for more details). Because both inward and outward prograde (retrograde) gravity waves transport energy toward the inside (outside) of the radiative layer, the two contributions act in concert and lead to the same change in the rotation of the radiative zone. The total tidal torque then leads to the following tidal dissipation:

$$|\mathfrak{J}(k_2)| = \frac{3^{-\frac{1}{3}} \Gamma^2\left(\frac{1}{3}\right)}{4\pi} m [l(l+1)]^{-\frac{4}{3}} \frac{\omega^{\frac{8}{3}} GM_\star^2}{n^4 m_p^2 R_\star^5} \times \left( \rho_0(r_{\text{int},1}) r_{\text{int},1} \left| \frac{dN^2}{d \ln r} \right|_{r_{\text{int},1}}^{-\frac{1}{3}} \mathcal{F}_{\text{out}}^2 + \rho_0(r_{\text{int},2}) r_{\text{int},2} \left| \frac{dN^2}{d \ln r} \right|_{r_{\text{int},2}}^{-\frac{1}{3}} \mathcal{F}_{\text{in}}^2 \right), \quad (135)$$

with

$$\mathcal{F}_{\text{out}} = \int_0^{r_{\text{int},1}} \left[ \left( \frac{r^2 \varphi_T}{g_0} \right)'' - \frac{l(l+1)}{r^2} \left( \frac{r^2 \varphi_T}{g_0} \right) \right] \frac{X_{1,\text{out}}}{X_{1,\text{out}}(r_{\text{int}})} dr, \quad (136)$$

$$\mathcal{F}_{\text{in}} = \int_{r_{\text{int},2}}^{R_\star} \left[ \left( \frac{r^2 \varphi_T}{g_0} \right)'' - \frac{l(l+1)}{r^2} \left( \frac{r^2 \varphi_T}{g_0} \right) \right] \frac{X_{1,\text{in}}}{X_{1,\text{in}}(r_{\text{int}})} dr.$$

From the boundary conditions we considered in Sects. 4 and 5.1, the functions  $X_{1,\text{in}}$  and  $X_{1,\text{out}}$  are solutions of the following Cauchy problems:

$$\begin{cases} X''_{1,\text{out}} - \frac{\partial_r \rho_0}{\rho_0} X'_{1,\text{out}} - \frac{l(l+1)}{r^2} X_{1,\text{out}} = 0 \\ X_{1,\text{out}}(0) = X'_{1,\text{out}}(0) = 0, \end{cases} \quad (137)$$

$$\begin{cases} X''_{1,\text{in}} - \frac{\partial_r \rho_0}{\rho_0} X'_{1,\text{in}} - \frac{l(l+1)}{r^2} X_{1,\text{in}} = 0 \\ X_{1,\text{in}}(R_\star) = X'_{1,\text{in}}(R_\star) = 0. \end{cases} \quad (138)$$

## 5. Variation in tidal dissipation of low-mass stars throughout their evolution

### 5.1. Physical insight and the *Goldreich & Nicholson (1989)* approach

We assumed that the totality of the energy flux carried by internal gravity waves is dissipated before the waves undergo any reflection. Therefore, tidal dissipation is directly linked to the efficiency of the excitation of the waves. Furthermore, in the

radiative zone, near the interface, the forced oscillations follow the inhomogeneous Airy equation

$$\frac{d^2 \psi}{d\eta^2} + v^2 \eta \psi = v^2 \eta Z, \quad (139)$$

with

$$v^2 = \frac{l(l+1)}{r_{\text{int}}^2 \omega^2} \left| \frac{dN^2}{dr} \right|_{r_{\text{int}}} \quad (140)$$

and

$$\eta = r_{\text{int}} - r. \quad (141)$$

We can therefore introduce a characteristic length  $\lambda$  of the variation in the gravity waves in the radial direction (*Goodman & Dickson 1998; Kushnir et al. 2017*), defined as

$$\lambda = v^{-\frac{2}{3}} = \omega^{\frac{2}{3}} [l(l+1)]^{-\frac{1}{3}} \left| \frac{dN^2}{d \ln r} \right|_{r_{\text{int}}}^{-\frac{1}{3}} r_{\text{int}}. \quad (142)$$

By following *Goldreich & Nicholson (1989)*, for a given forcing frequency  $\omega$ , the group velocity  $v_g$  of the gravity waves can then be estimated as  $v_g \sim \lambda \omega$ . Furthermore, because gravity waves are excited by the equilibrium tide, the characteristic velocity  $u$  of the fluid can be assessed as  $u \sim \xi_{\text{eq,int}} \omega$ , where  $\xi_{\text{eq,int}} \sim -\frac{\varphi_T(r_{\text{int}})}{g_{0,\text{int}}}$  (*Zahn 1975*) is the radial displacement linked to the equilibrium tide estimated at the interface. The energy luminosity  $L_E$  can therefore be expressed as

$$\begin{aligned} L_E &\sim \rho(r_{\text{int}}) u^2 v_g r_{\text{int}}^2 \\ &= \rho(r_{\text{int}}) \lambda \omega^3 r_{\text{int}}^2 \left( \frac{\varphi_T(r_{\text{int}})}{g_{0,\text{int}}} \right)^2. \end{aligned} \quad (143)$$

By introducing  $\varphi_T(r_{\text{int}}) = r_{\text{int}}^2 \Psi$  and  $\omega_{\text{dyn,int}}^2 = g_{0,\text{int}}/r_{\text{int}}$ , we obtain

$$L_E \sim \omega^{\frac{11}{3}} \rho(r_{\text{int}}) r_{\text{int}}^5 \left| \frac{dN^2}{d \ln r} \right|_{r_{\text{int}}}^{-\frac{1}{3}} \left( \frac{\Psi}{\omega_{\text{dyn,int}}^2} \right)^2, \quad (144)$$

which is similar to the *Goodman & Dickson (1998)* formulation, as was pointed out by *Kushnir et al. (2017)* and in our prescription. The tidal dissipation then becomes

$$\begin{aligned} |\mathfrak{J}(k_2)| &\propto \frac{GM_\star^2}{m_p^2 R_\star^5} \frac{1}{n^4} \frac{L_E}{\omega} \\ &\propto \frac{\omega^{\frac{8}{3}} GM_\star^2}{n^4 m_p^2 R_\star^5} \rho_0(r_{\text{int}}) r_{\text{int}} \left| \frac{dN^2}{d \ln r} \right|_{r_{\text{int}}}^{-\frac{1}{3}} \left( \frac{\Psi}{\omega_{\text{dyn,int}}^2} \right)^2. \end{aligned} \quad (145)$$

This approach allows us to better understand the effect of the relevant physical parameters on tidal dissipation. For a given star-planet system, a higher density at the interface will increase the energy carried by the waves and therefore the tidal dissipation. A similar effect can be obtained for higher values of  $r_{\text{int}}$  and smoother slopes of the Brunt-Väisälä profile, which enhance the group velocity.

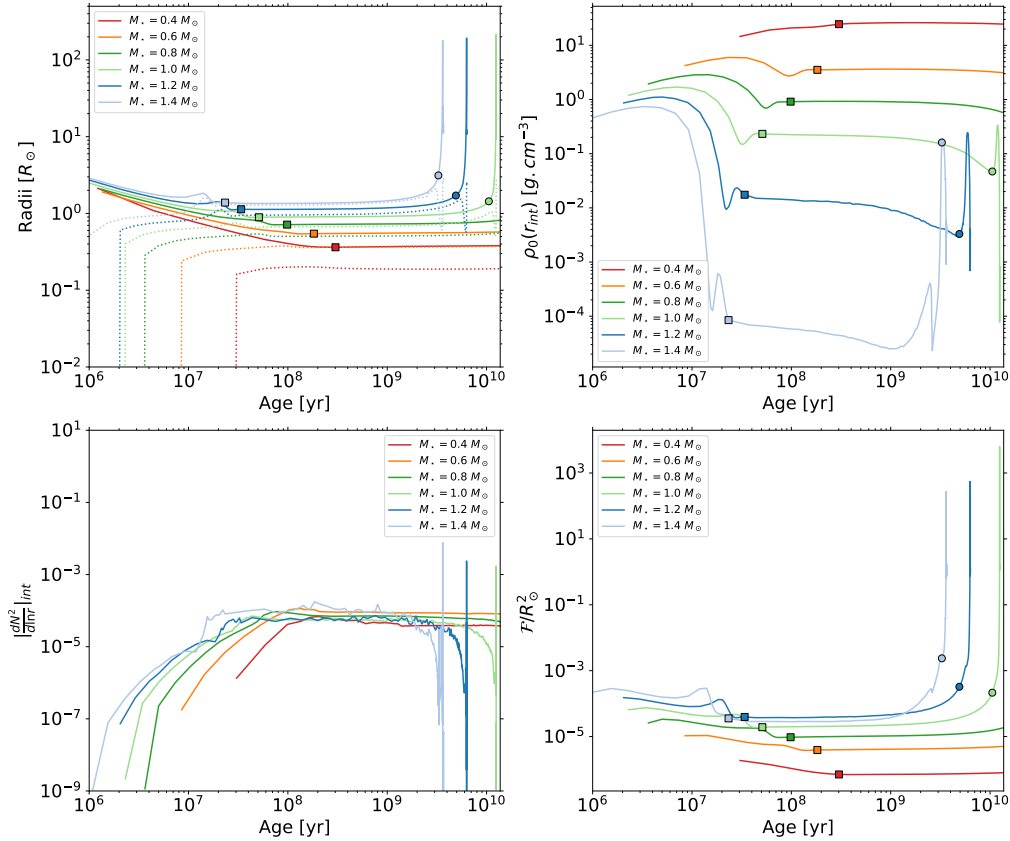


**Fig. 4.** Evolution of the stellar radius (*top left*, plain line), the radius of the radiative zone (*top left*, dotted line), the density at the interface core-envelope (*top right*), the gradient of the square of the Brunt–Väisälä frequency at the interface (*bottom left*) and the forcing term  $\mathcal{F}$  (*bottom right*) as a function of the age of the system for stellar masses ( $M_*$ ) between 0.4 and  $1.4 M_\odot$ , with  $P_{\text{orb}} = 1$  d, a typical value for a hot Jupiter. The colored squares correspond to the ZAMS in each model, and the colored circles represent the TAMS.

## 5.2. Model grid for low-mass stars

To study the effect of stellar structure and evolution on tidal dissipation in the radiative zone of low-mass stars, we relied on grids computed with the 1D stellar evolution code STAREVOL (see [Siess et al. 2000](#); [Lagarde et al. 2012](#); [Amard et al. 2019](#), for an extensive description) for masses ranging from 0.4 to  $1.4 M_\odot$  at solar metallicity  $Z = 0.0134$  ([Asplund et al. 2009](#)). We studied all phases from the PMS to the top of the RGB.

As shown in [Fig. 4](#) (top left panel), the star is completely convective at the beginning of the evolution and then contracts during the PMS. A radiative core grows after the Hayashi phase, and a mass transfer occurs from the convective envelope to the radiative zone, leading to an increase and then a decrease in density at the core-envelope interface during the PMS (top right panel). At the zero-age main sequence (ZAMS), the stellar radius, the size of the radiative core, and the density at the core-envelope interface reach a value that remains almost constant during the MS. There, the thinner convective envelope of more massive stars lead to lower densities at the interface. During the subgiant phase, low-mass stars are characterized by larger radii, thicker convective layers, and higher densities at the interface than their MS counterparts because the envelope expands and the core contracts.

A key contribution for assessing tidal dissipation in low-mass stars is the forcing term

$$\mathcal{F} = \int_{r_{\text{int}}}^{R_*} 6 \left(1 - \frac{\rho}{\bar{\rho}}\right) \left[ \frac{1}{r} \left( \frac{r^2 \varphi_T}{g_0} \right)' - \frac{2}{r^2} \left( \frac{r^2 \varphi_T}{g_0} \right) \right] \frac{X_1}{X_1(r_{\text{int}})} dr. \quad (146)$$

At a given age, this quantity is computed by relying on the density radial profiles provided by STAREVOL in order to obtain the solution  $X(r)$  in the convective envelope. Below the stellar surface, the density profile is replaced by a polytropic model, whose polytropic index varies with the extent of the convective zone to ensure a singularity at  $r = R_*$  (for more details about the numerical implementation of surface boundary conditions, we refer to [Eq. \(C.5\)](#)). The differential equations were solved by relying on a fourth-order Runge–Kutta method. In this way, if we neglect the changes in stellar structure, [Eq. \(127\)](#) leads to  $\mathcal{F} \propto R_*^5 M_*^{-1}$  for a given star–planet system (which allows us to keep the tidal potential constant). According to this scaling law, the forcing term presents a time evolution similar that of to the stellar radius (see the bottom right panel in [Fig. 4](#)). Furthermore, when we consider a mass–radius relationship during the MS, the  $\mathcal{F}$  term tends to be higher for more massive stars. However, taking an inhomogeneous distribution of mass in the stellar interior and variations in stellar structure into account, we find a more complex behavior of the forcing term  $\mathcal{F}$ . For  $M_* = 1.4 M_\odot$ ,  $\mathcal{F}$  reaches higher values than for the  $1.2 M_\odot$  evolution at the beginning of the PMS and during the SG phase. However, at the end of the PMS and during the MS, a reduced contribution of the forcing term can be seen for  $M_* = 1.4 M_\odot$ .

Despite a noisy profile inherent to the numerical treatment of the stellar interior, the bottom left panel in [Fig. 4](#) shows that the gradient of the squared Brunt–Väisälä frequency increases during the PMS. It then reaches a stationary value on the MS, which does not depend on the stellar mass. In this way, its main effect is to enhance tidal dissipation in young systems. This behavior

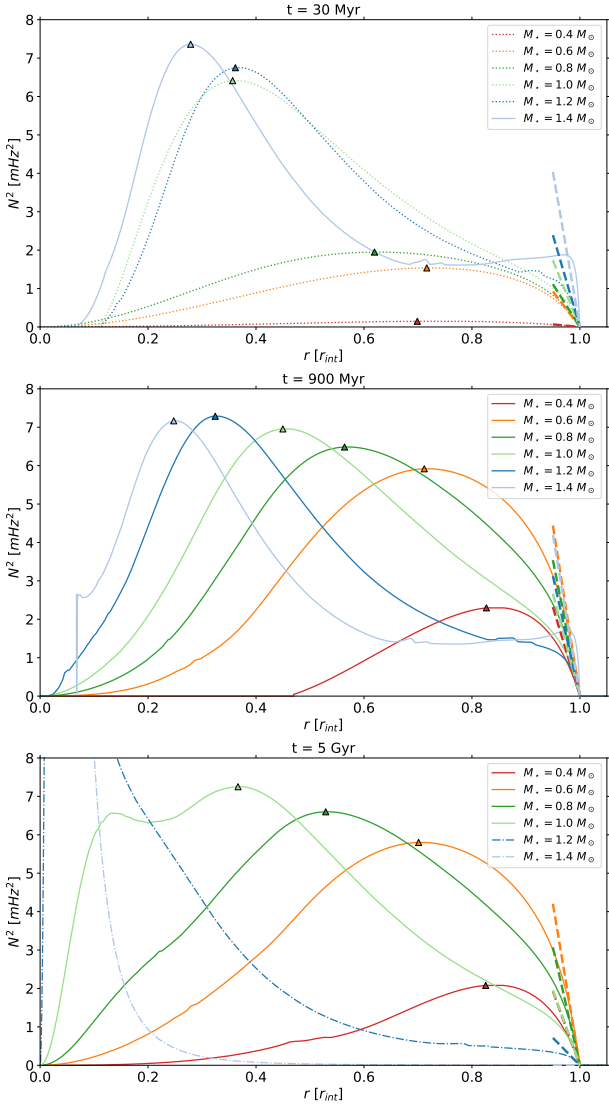


**Fig. 5.** Brunt–Väisälä frequency profiles as a function of the distance to the center of the star, normalized to the radius of its radiative zone, at 30 Myr (*top panel*), 900 Myr (*middle panel*), and 5 Gyr (*bottom panel*). The dotted profiles are situated in the PMS, the plain lines in the MS, and the dash-dotted lines in the post-MS phase. The colors correspond to the same stellar masses as in Fig. 4. The dashed lines correspond to the tangents to the  $N^2$  profiles at the interface. The triangles indicate the position of the maximum Brunt–Väisälä frequency.

can be explained by considering the evolution of the Brunt–Väisälä profiles for different stellar masses. As shown in Fig. 5, the Brunt–Väisälä frequency drops at the center and at the interface between the convective and the radiative zones at all ages. Moreover, during the PMS (see the dotted lines in Fig. 5), the frequency at a given radius increases due to the contraction of the star, which locally increases the gravity (Charbonnel et al. 2013). This leads to higher maximum values of  $N^2$  during the early evolution. Furthermore, because

$$\left. \frac{dN^2}{d \ln r} \right|_{\text{int}} = \left. \frac{dN^2}{d \left( \frac{r}{r_{\text{int}}} \right)} \right|_{\text{int}}, \quad (147)$$

it also explains the increase in the gradient of  $N^2$  at the interface during the PMS. During the MS (see the plain lines in Fig. 5),

as the structure of the star is stabilized, the position of the maximum frequency in the radiative zone approaches the center of the evolving star. This marginally changes its value and the general shape of the profile. Thus  $dN^2/d \ln r$  and  $N_{\text{max}}$  remain approximately constant during this phase. The dependence on stellar mass of these two quantities is then essentially explained by the relative PMS and MS lifetimes of the different types of stars. The more massive the star, the faster its PMS evolution, and thus the earlier the  $dN^2/d \ln r$  and  $N_{\text{max}}$  values reach the MS plateau. During the subgiant phase and the RGB (see the dash-dotted lines in Fig. 5), as the maximum value of  $N^2$  increases and approaches the center of the star (Fuller et al. 2014), the gradient  $dN^2/d \ln r$  at the convective–radiative interface decreases, which emphasizes tidal dissipation in the radiative zone.

### 5.3. Time evolution of tidal dissipation as a function of stellar mass and evolutionary stage

The evolution of our tidal dissipation prescription (see the green curve in the top panels of Fig. 6) for a planet orbiting a nonrotating star with a period  $P_{\text{orb}} = 1$  d is similar to the prescriptions of Barker & Ogilvie (2010; dashed black line in the top panels of Fig. 6) and Goodman & Dickson (1998; dotted black line in the top panels of Fig. 6). The discrepancies between these estimates of tidal dissipation come from the parametrization of  $dN^2/d \ln r$  and  $d\xi_r/dr$  at the core–envelope interface, which are sensitive to the hypothesis made in a given stellar evolution model. The simplified version of our prescription, derived in Sect. 4.2.3 (see the green dashed curve in the top panels of Fig. 6) is only relevant during the MS of higher-mass stars, where the thin convective layer approximation remains valid.

The bottom panels in Fig. 6 show that tidal dissipation increases at the beginning of the PMS toward its maximum value because a radiative core forms. This maximum increases with stellar mass and is reached earlier for more massive stars because their lifetime is shorter. The energy transported by IGW is then reduced by the decrease in density at the interface that is due to mass transfer from the envelope to the core, and to a lesser extent, by an increase in the gradient of the Brunt–Väisälä frequency. Their excitation is then inhibited and tidal dissipation decreases to reach an almost constant value during the MS. During this evolutionary stage, G-type and K-type stars ( $M_{\star} = \{0.6 - 1\} M_{\odot}$ ) present a similar dissipation, as was pointed out by Barker (2020). In the case of F-type stars ( $M_{\star} = \{1.2 - 1.4\} M_{\odot}$ ), tidal dissipation decreases by about four orders of magnitude as the stellar mass increases and the convective envelope becomes thinner. It is important to note that for these stars, the dissipation of progressive waves probably is not the dominating contribution to tidal friction in the stellar radiative zone because standing modes may undergo a more efficient dissipation that is enhanced through resonance locking (Fuller 2017). For M-type stars (here  $M_{\star} = 0.4 M_{\odot}$ ), the smaller extension of the radiative core leads to a weaker tidal dissipation. At the end of the MS phase, as the hydrogen is mostly consumed, the core becomes isothermal and contracts. At the same time, the remaining burning hydrogen migrates to form a shell around the helium core. This leads to an inflation of the convective envelope. As the density at the interface increases, the tidal dissipation therefore becomes stronger during the subgiant phase and the RGB.

This evolution of tidal dissipation as a function of stellar mass and stellar age is expected when  $\omega < \omega_c$ , when an interaction with a corotation layer occurs, or when wave braking develops within the radiative core. For this last mechanism, the mass of the companion has to be greater than a critical value

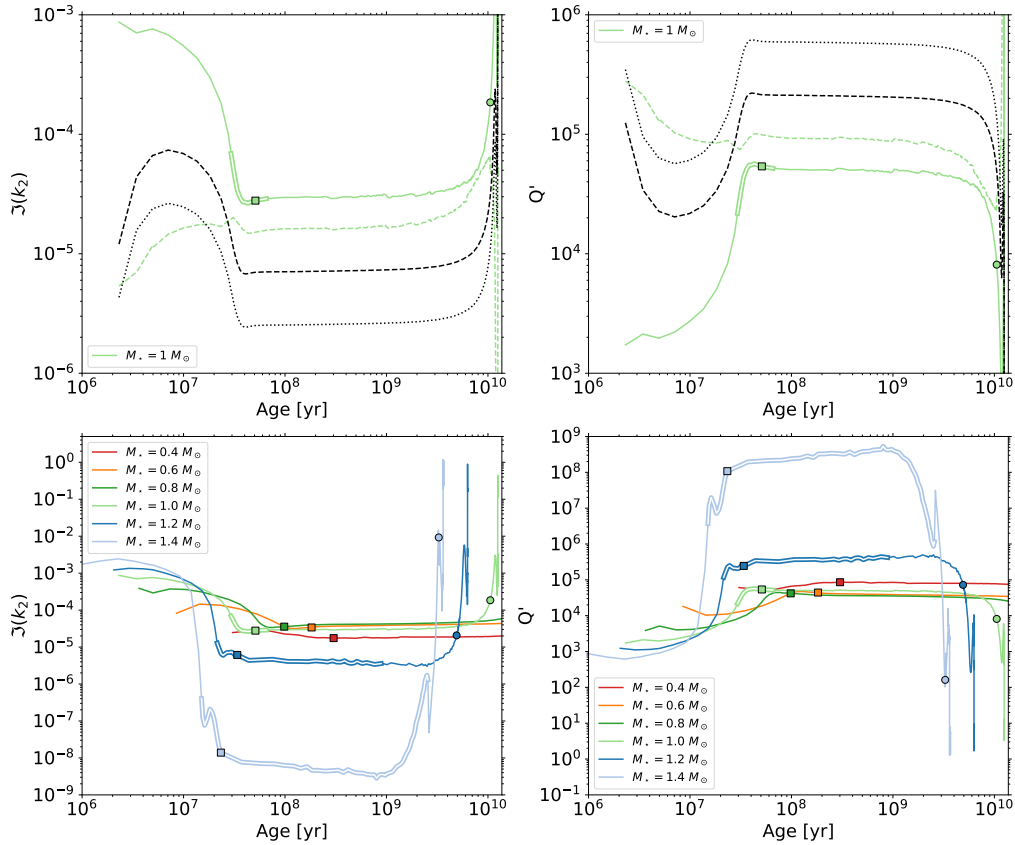


**Fig. 6.** Evolution of the tidal dissipation and the corresponding quality factor as a function of stellar mass and stellar age. *Top left:* evolution of the tidal dissipation as a function of time for  $M_{\star} = 1 M_{\odot}$  and  $P_{\text{orb}} = 1$  d. *Top right:* time evolution of the corresponding tidal quality factor. In green we plot the prescription developed in our work. Dashed green shows the simplified prescription for a thin convective envelope. The dashed black line shows the [Barker & Ogilvie \(2010\)](#) prescription. The dotted black line represents the [Goodman & Dickson \(1998\)](#) prescription. *Bottom left:* evolution of the tidal dissipation as a function of time for stellar masses ( $M_{\star}$ ) between 0.4 and  $1.4 M_{\odot}$ , with  $P_{\text{orb}} = 1$  d. *Bottom right:* time evolution of the corresponding tidal quality factor. The colored squares correspond to the ZAMS and the colored circles to the TAMS in each model. Double lines indicate the presence of a convective core. In this configuration, wave braking is unlikely to occur.

$M_{\text{cr}}$  (we refer to Appendix D, and [Barker & Ogilvie 2010](#); [Barker 2011, 2020](#) for more details). In particular, during the subgiant phase and the RGB, more massive stars require lower planetary masses to initiate wave breaking. This means that super-Earths and hot Neptunes are likely to trigger this process during these phases of evolution because the convective envelope of the star is thicker (see Appendix D and [Barker 2020](#)).

#### 5.4. Dynamical tide in the convective and the radiative zones of low-mass stars: effect of structural and rotational evolution

We aim in this section to compare the dissipation of the dynamical tide in the radiative and convective zones of low-mass stars throughout their evolution. In particular, we take the evolution of stellar rotation into account to assess the dissipation of tidal inertial waves in the convective layer. We then study the effect of metallicity and stellar structure (bilayer versus trilayer) on the tidal dissipation through gravity waves.

##### 5.4.1. Spin evolution

A consistent treatment of the tidal dissipation in the convective zone requires taking the evolution of stellar rotation into account. To this end, we relied on STAREVOL evolutionary tracks adapted from [Amard et al. \(2019\)](#). We computed stellar models of rotating stars for a range of initial masses between

0.4 and  $1.4 M_{\odot}$  at solar metallicity. The star–disk interaction was taken into account at the beginning of the PMS by assuming a constant surface rotation rate during the disk lifetime, set by the observations. Over the whole mass range, we selected the fast rotators as calibrated by [Gallet & Bouvier \(2015\)](#) with a three-day initial rotation period and a 2.5 Myr disk lifetime. In this way, we considered an upper bound of the tidal dissipation through inertial waves.

Figure 7 shows that after the dissipation of the disk, the star spins up during the PMS due to its contraction. During the MS, the magnetized stellar winds then carry angular momentum away from the star, leading to its spin-down ([Skumanich 1972](#); [Kawaler 1988](#); [Matt et al. 2015](#)). As the evolution of the most massive stars is faster than that of the least massive, the decrease in their rotation rate at the beginning of the MS occurs at lower ages. Furthermore, F stars have a smaller outer convective zone, leading to a less efficient stellar dynamo. They are therefore less strongly braked during the MS and thus remain fast rotators during most of their life. Therefore lower-mass stars reach a slower rotation rate at the solar age than their higher-mass counterparts.

##### 5.4.2. Tidal dissipation in the convective zone

We now aim to compare the dissipation of the dynamical tide in the radiative and convective zones of low-mass stars

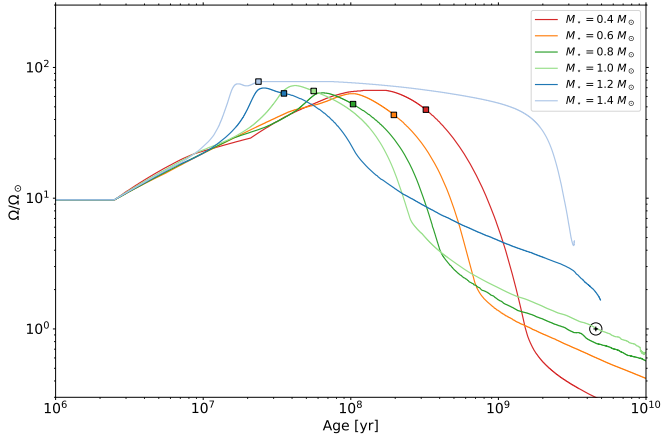


**Fig. 7.** Evolution of the surface rotation rate (scaled to the present Sun rotation rate) for stars with a mass ranging from 0.4 to 1.4 solar masses (Amard et al. 2019). The solar rotation rate at solar age is represented by a black circle. The colored squares correspond to the ZAMS in each model.

throughout their evolution. To this end, we relied on the formalism of Ogilvie (2013) and Mathis (2015) to assess tidal dissipation in the convective zone through inertial waves. In this framework, we assumed the same simplified bilayer structure as in Sect. 5.3. The stellar convective envelope was assumed to be in solid-body rotation with angular velocity  $\Omega_*$ . Furthermore, centrifugal effect was neglected by assuming moderate rotation, that is,  $\Omega_*^2/\omega_{\text{dyn}}^2 \ll 1$ . In the case of a coplanar and circular star-planet system, the frequency-averaged tidal dissipation is given by

$$\begin{aligned} \langle \mathfrak{J}(k_2) \rangle_{\text{IW}}^{\text{CZ}} &= \int_{-\infty}^{+\infty} \mathfrak{J}(k_2) \frac{d\omega}{\omega} = \frac{100\pi}{63} \left( \frac{\Omega_*}{\omega_{\text{dyn}}} \right)^2 \left( \frac{\alpha^5}{1-\alpha^5} \right) (1-\gamma)^2 \\ &\times (1-\alpha)^4 \left( 1 + 2\alpha + 3\alpha^2 + \frac{3}{2}\alpha^3 \right)^2 \left[ 1 + \left( \frac{1-\gamma}{\gamma} \right) \alpha^3 \right] \\ &\times \left[ 1 + \frac{3}{2}\gamma + \frac{5}{2\gamma} \left( 1 + \frac{1}{2}\gamma - \frac{3}{2}\gamma^2 \right) \alpha^3 - \frac{9}{4}(1-\gamma)\alpha^5 \right]^{-2}, \end{aligned} \quad (148)$$

with  $\alpha = \frac{R_r}{R_*}$ ,  $\beta = \frac{M_r}{M_*}$  and  $\gamma = \frac{\rho_c}{\rho_r} = \frac{\alpha^3(1-\beta)}{\beta(1-\alpha^3)}$ ,  $R_r$  being the radius of the radiative zone and  $M_r$  its mass. The effective calculation of the tidal dissipation related to the excitation of inertial modes leads to a strongly frequency-dependent resonant spectrum that is highly sensitive to the friction in the stellar medium (Savonije & Papaloizou 1997; Ogilvie 2013). A frequency average then provides a reasonable estimate likely to over- or underestimate the effective dissipation at a given frequency. Moreover, the assumption of a bilayer structure for the star is reasonable for stellar masses lower than 1.2  $M_\odot$  because the Mathis (2015) prescription underestimates tidal dissipation by a factor lower than 2 compared to the Ogilvie (2013) formulation applied to a more realistic stratified structure of the star (Barker 2020). However, in the case of F-type stars, the two-layer model may generally underpredict the dissipation by at least one order of magnitude.

Furthermore, the dissipation of the equilibrium tide in the convective zone can be estimated as (Remus et al. 2012)

$$\langle \mathfrak{J}(k_2) \rangle_{\text{eq}}^{\text{CZ}} = 4\pi \frac{2088}{35} \frac{R_*^4}{GM_*^2} \left| \omega \int_{\alpha}^1 x^8 \rho_{\text{CZ}} \nu_t dx \right|, \quad (149)$$

where  $\nu_t$  is the turbulent viscosity in the convection zone,  $\rho_{\text{CZ}}$  is the density in the convection zone, and  $x = r/R_*$  is the normalized radial coordinate. Following Duguid et al. (2020), the turbulent viscosity strength can be assessed from the convective turnover time  $t_c$  as

$$\nu_t = \nu_c l_c F(\omega), \quad (150)$$

where  $\nu_c$  is the typical convective velocity,  $l_c$  is the mixing length, and

$$F(\omega) = \begin{cases} 5, & |\omega|t_c < 10^{-2} \\ \frac{1}{2} (|\omega|t_c)^{-\frac{1}{2}}, & |\omega|t_c \in [10^{-2}, 5] \\ \frac{25}{\sqrt{20}} (|\omega|t_c)^{-2}, & |\omega|t_c > 5. \end{cases} \quad (151)$$

This prescription accounts for the results of the latest numerical simulations of the interaction between turbulent convection and tidal flows. In particular, they provide strong evidence in favor of the Goldreich & Nicholson (1989) frequency dependence at high frequencies because the energetically dominant modes of the convection contribute most to the effective viscosity (for a more in-depth discussion, we refer to Barker 2020). As we only aim here to provide an order of magnitude of tidal dissipation, we assumed a constant density in the convective zone equal to  $\rho_{\text{CZ}} = 3M_*(1-\beta)/4\pi R_*^3(1-\alpha^3)$ . Furthermore, we approximated the mixing length  $l_c$  by its maximum, given by the depth of the convective zone  $(1-\alpha)R_*$ . This leads to

$$[\mathfrak{J}(k_2)]_{\text{eq}}^{\text{CZ}} = \frac{696}{35} |t_c \omega| \frac{R_*}{GM_*} \nu_c^2 (1-\beta) \frac{1-\alpha^9}{1-\alpha^3} F(\omega). \quad (152)$$

Given the stellar luminosity  $L_*$  and the rotation period  $P_{\text{rot}}$ , we can estimate the convective velocity  $\nu_c$  and convective turnover time  $t_c$  from the Mathis et al. (2016) formulation based on the mixing-length theory for a rotating body (e.g., Stevenson 1979; Augustson & Mathis 2019),

$$\nu_c = \nu_{c,0} \begin{cases} \left( 1 - \frac{1}{242Ro^2} \right), & Ro > 0.25 \\ 1.5 Ro^{\frac{1}{5}}, & Ro < 0.25, \end{cases} \quad (153)$$

where  $Ro = P_{\text{rot}} \nu_{c,0} / l_c$  is the convective Rossby number and  $\nu_{c,0} = (L_*/(\rho_{\text{CZ}} R_*^2))^{1/3}$  is the convective velocity from the standard mixing-length theory, without rotation. For both prescriptions, we relied on STAREVOL to compute the stellar mass, radius, rotation, and luminosity and to assess the  $\alpha, \beta$  coefficients. Furthermore, we chose the so-called conventional equilibrium tide (Zahn 1966; Remus et al. 2012), which is defined as the hydrostatic response of the star to the tidal potential. Its use in convective zone is discussed in favor of a non-wavelike equilibrium tide (Goodman & Dickson 1998; Terquem et al. 1998; Ogilvie 2014). However, as presented in Barker (2020), the first formulation differs from the second by a factor of 2–3. This discrepancy does not affect our results because we considered both orders of magnitudes and upper bounds of tidal dissipation.

#### 5.4.3. Comparison with tidal dissipation in the convective envelope throughout stellar evolution

We now compare tidal dissipation in the stellar radiative and convective zones throughout stellar evolution. To do so, we first need

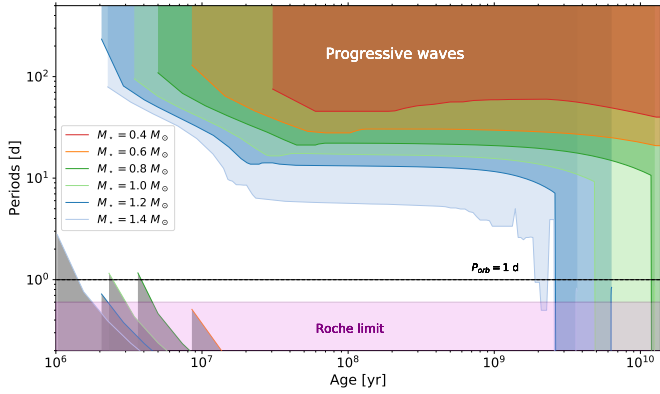


**Fig. 8.** Characteristic periods as a function of the age of the system for stellar masses between 0.4 and  $1.4 M_{\odot}$ . In dark gray we plot the region corresponding to tidal frequencies greater than  $N_{\max}$ , for which no propagation of gravity waves is allowed. The colored areas correspond to orbital periods that are likely to excite progressive waves (with frequencies  $\omega < \omega_c$ ) for each stellar mass. In purple we show typical values corresponding to the Roche limit. The dashed black line corresponds to an orbital period of one day.

to study the frequencies available to tidal gravity waves as a function of stellar mass and stellar age. For tidal frequencies higher than the maximum Brunt–Väisälä frequency  $N_{\max}$ , the propagation of internal gravity waves is not allowed (the corresponding periods are represented as gray areas in Fig. 8). However, this case in general corresponds to orbital periods below the Roche limit (in violet in the same figure; for a calculation of this limit, we refer to Benbakoura et al. 2019). This implies that after several million years of evolution, a planet is likely to excite gravity waves throughout the evolution of the star for all the stellar masses considered.

Figure 8 also represents the orbital period corresponding to the cutoff frequency  $\omega_c$ . Beyond this critical period, tidal gravity waves are entirely dissipated through radiative damping before undergoing any reflection (see the colored regions in Fig. 8). As stratification and thermal diffusivity are higher for the most massive and the oldest stars, close-in planets are more likely to excite progressive waves in the radiative zone of this type of stars. During the RGB, even planets located at the Roche limit are therefore able to excite progressive waves. During the PMS and MS of the least massive stars, a planet excites gravity waves that cannot be entirely dissipated through radiative damping. In the absence of other ways of dissipation,  $g$ -modes are then formed. However, for sufficiently massive planets, wave breaking may occur at the center of the star, or in the presence of differential rotation, gravity waves may interact with a critical layer. In this case, close-in planets may generate efficient tidal dissipation in the stellar radiative zone.

To evaluate an order of magnitude of the contribution of the dissipation of tidal gravity waves, it might be tempting to rely on the method introduced by Ogilvie (2013), Mathis (2015), and Gallet et al. (2017) for tidal inertial waves. They computed a frequency average that would evaluate the capacity of a given stellar structure to dissipate the tidal wave, assuming that it is excited in an impulsive way and is dissipated after a finite time by a dissipation mechanism. We would then have

$$\langle \mathfrak{J}(k_2) \rangle_{\text{IGW}}^{\text{RZ}} = \int_0^{\omega_c} \mathfrak{J}(k_2) \frac{d\omega}{\omega}, \quad (154)$$

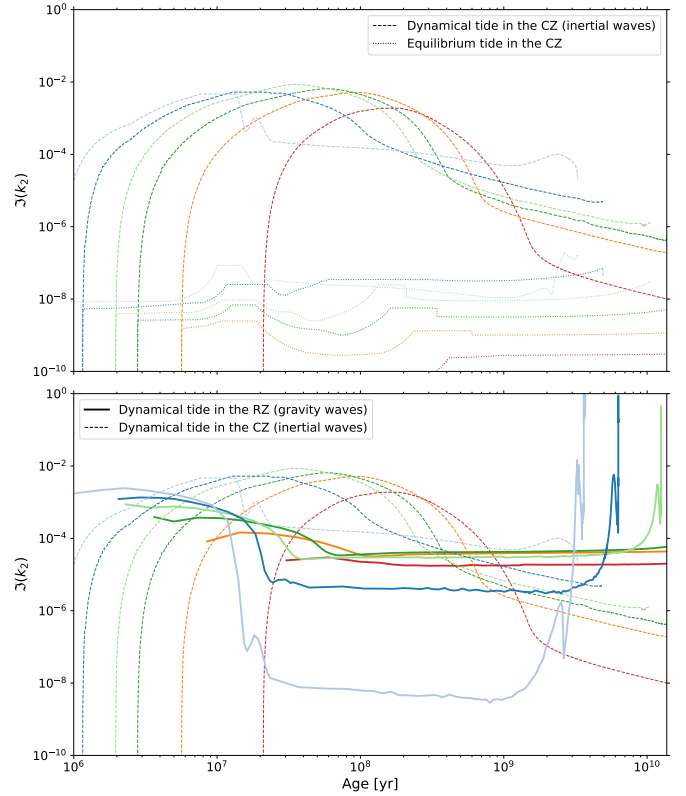


**Fig. 9.** *Top:* evolution of the dissipation of the dynamical tide through inertial waves (dashed lines) and of the equilibrium tide in the convective zone (dotted lines). *Bottom:* evolution of the dissipation of the dynamical tide through gravity waves (solid lines) and of the dynamical tide through inertial waves (dashed lines). Stellar mass ranges between 0.4 and  $1.4 M_{\odot}$ . The colors correspond to the same masses as in Fig. 8.

which for solar-type stars gives

$$\langle \mathfrak{J}(k_2) \rangle_{\text{IGW}}^{\text{RZ}} = \frac{3^{\frac{2}{3}} \Gamma^2 \left( \frac{1}{3} \right)}{32\pi} |m| [l(l+1)]^{\frac{1}{2}} \frac{GM_{\star}^2}{R_{\star}^5} \omega_{\text{conv}} \times \rho_0(r_{\text{int}}) r_{\text{int}} \left| \frac{dN^2}{d \ln r} \right|_{r_{\text{int}}}^{-\frac{1}{3}} \frac{\mathcal{F}^2}{m_p^2 n^4}. \quad (155)$$

We stopped the frequency average at  $\omega_c$  because we focus on progressive waves.

However, the frequency-averaged method is meaningful in the case of a strongly resonant and erratic dissipation. For instance, in the case of tidal inertial waves, the amplitude of the resonant dissipation strongly depends on the strength of the turbulent friction applied by convection (Ogilvie & Lin 2004, 2007; Auclair-Desrotour et al. 2015; Mathis et al. 2016). However, we cannot use this approach if the dissipation varies with a power law of the tidal frequency, as is the case for progressive gravity waves (the same holds for the equilibrium tide). In this configuration, the frequency-averaged dissipation would lead to a lower bound that is not representative. We therefore chose an effective evaluation for a typical hot-Jupiter system with a period of one day.

Figure 9 shows the evolution of the dissipation of the equilibrium tide in the convective zone (dashed lines) and of the dynamical tide through inertial waves (dashed lines) and gravity waves (solid lines) for  $M_{\star} = 0.4 - 1.4 M_{\odot}$ . The dissipation of the

equilibrium tide in the radiative zone is neglected here because its efficiency is much lower than the other contributions (Zahn 1966, 1977). Moreover, because we considered fast rotators, the dissipation through inertial waves that we calculated acts as an upper bound. While the tidal dissipation through gravity waves is comparable to its counterpart in the convective zone at the beginning of PMS, the mass transfer from the convective to the radiative zone decreases the efficiency of the dissipation in the stellar core, as presented in Sect. 5.3. This means that during most of the PMS and the beginning of the MS, when the rotation of the star is at its highest, the dissipation of the dynamical tide in the convective zone dominates. The dissipation of the equilibrium tide is then lower by several orders of magnitude than the other two contributions.

Because magnetic braking substantially decreases the stellar rotation rate, the tidal dissipation through inertial waves during the MS loses efficiency to the benefit of the dissipation in the core. This dissipation remains constant during the MS due to the small changes in stellar structure. During the most advanced phases, the equilibrium tide becomes comparable to the contribution of inertial waves. In the case of the most massive stars, the equilibrium tide is likely to become the dominant contribution within the stellar envelope. This scenario is consistent with the evolution of eccentricities observed for red giant binaries observed by the *Kepler* mission (Beck et al. 2018). However, because the core contracts and the envelope expands during the SG phase and the RGB, tidal dissipation through gravity waves becomes largely dominant. This may have a strong effect on the secular evolution of star–planet systems and binaries during the most advanced phases (Schlaufman & Winn 2013; Essick & Weinberg 2016; Weinberg et al. 2017; Vick & Lai 2020). When slower rotators (with a rotation period between 5 and 10 days) are considered, the tidal dissipation through inertial waves is less efficient, as  $\mathfrak{J}[k_2] \propto \Omega_\star^2$ . The dissipation through gravity waves then dominates the evolution of the system during longer phases, at the beginning of the PMS and at the end of MS.

### 5.5. Effect of stellar metallicity

Stellar metallicity may affect the secular evolution of star–planet systems and thereby the orbital period distribution of hot Jupiters (e.g., Gonzalez 1997; Santos et al. 2003). In order to assess its effect on tidal dissipation through gravity waves, we focused on a  $1 M_\odot$  star with three different metallicities, that is,  $Z = 0.004$ ,  $Z = 0.0134 = Z_\odot$ , and  $Z = 0.0255$ , as in Bolmont et al. (2017). When the metallicity of the star increases, its opacity evolves in the same way (Kippenhahn & Weigert 1994). This has the effect of decreasing the stellar luminosity and the effective temperature, which subsequently increases the overall lifetime of the star. Furthermore, the radiative zone shrinks, which causes the density at the convective–radiative interface to increase at a given evolutionary phase.

Figure 10 shows that tidal dissipation through gravity waves evolves in the same way, regardless of the stellar metallicity considered. Furthermore, dissipation increases along with metallicity. This behavior may lead to a discrepancy of about one order of magnitude near the ZAMS between the solar metallicity case ( $Z = 0.0134$ ) and the metal-poor case ( $Z = 0.004$ ). At the beginning of the evolution, metal-poor stars undergo a stronger dissipation than metal-rich stars. The higher the metallicity, the later the formation of the radiative core. As the radiative zone reaches its maximum extension at the end of the PMS, the opposite behavior is therefore observed, and dissipation increases with metallicity. At the end of evolution,

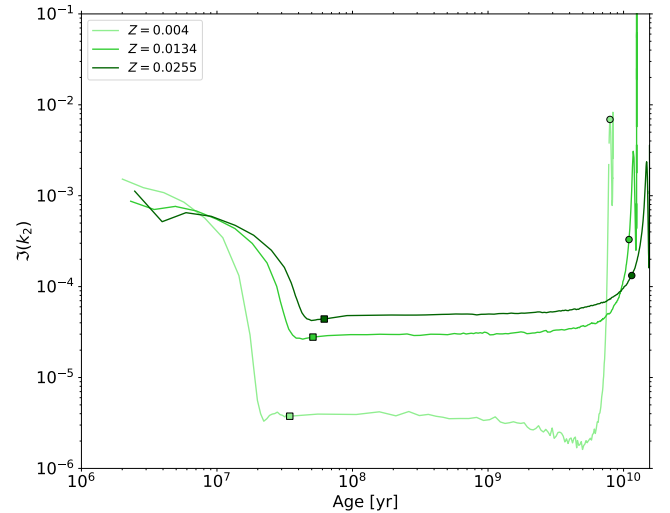


**Fig. 10.** Evolution of the tidal dissipation through gravity waves as a function of time for three different stellar metallicities, i.e.,  $Z = 0.004$ ,  $Z = 0.0134 = Z_\odot$ , and  $Z = 0.0255$ , with  $M_\star = 1 M_\odot$  and  $P_{\text{orb}} = 1$  d. The colored squares correspond to the ZAMS in each model, and the colored circles show the TAMS.

as metal-poor stars reach the subgiant phase and the RGB before their metal-rich counterparts, the observed trend reverses again and the dissipation of metal-poor stars becomes more efficient.

### 5.6. Tidal dissipation in massive solar-type stars: bilayer versus trilayer structure

We now focus on the STAREVOL models with stellar masses ranging from  $1$  to  $1.4 M_\odot$ . Figure 11 shows that all models form a convective core near the ZAMS. However, for  $M_\star = 1.4 M_\odot$ , the star maintains its core during the entire MS, while for  $M_\star = 1.2 M_\odot$  the core disappears at around 1 Gyr. For  $M_\star = 1 M_\odot$  the convective core only remains for 40 Myr.

In this configuration, as shown in Fig. 12, the contribution of a convective core to the total tidal dissipation is negligible compared to the contribution of the outer thin convective envelope we derive for a bilayer structure. Despite a higher density at lower radii, the low extent of the core tends to reduce tidal dissipation through outward gravity waves, especially with the aid of the forcing term  $\mathcal{F}$ . This contribution involves a  $(1 - \frac{\rho}{\bar{\rho}})$  factor, with  $\bar{\rho}$  the mean density inside a sphere of radius  $r$ , which in a core configuration quantifies the inhomogeneity of the mass distribution near the center. A tiny convective core, coupled with a flat mass distribution near the center from spherical symmetry, then leads to a weak dissipation.

## 6. Conclusions and discussions

We provided a general formalism for assessing tidal dissipation in stellar radiative zones in all types of stars. We focused on the angular momentum flux transported by progressive tidal gravity waves, which are more likely to affect the secular evolution of the considered binary or planetary system (Goodman & Dickson 1998; Terquem et al. 1998). This approach allowed us to gather the founding work of the Zahn (1975), Goldreich & Nicholson (1989), Goodman & Dickson (1998), and Barker & Ogilvie (2010) prescriptions, among others, into a unique flexible framework that is applicable to all types of

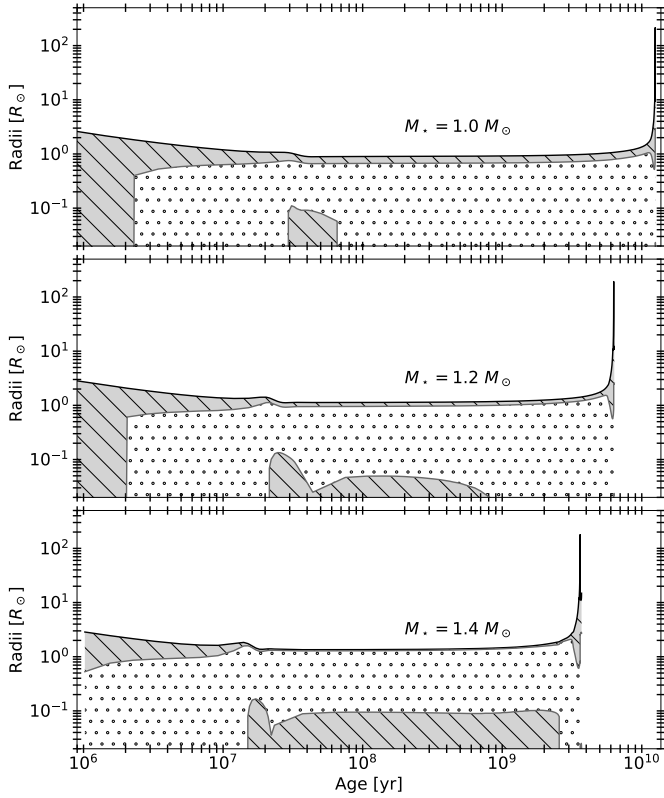


**Fig. 11.** Kippenhahn diagram showing the evolution of the internal structure of the nonrotating star for  $M_* = 1 M_\odot$  (top),  $M_* = 1.2 M_\odot$  (middle), and  $M_* = 1.4 M_\odot$  (bottom) from the PMS up to the end of the MS. The upper line represents the stellar radius in solar radii. The hatched gray areas depict convective regions, and the dotted areas stand for radiative regions.

stars and planetary systems. In the case of low-mass stars, we investigated the effect of stellar structure and evolution on tidal dissipation through gravity waves. We showed that for a given star–planet system, tidal dissipation reaches a maximum value on the PMS for all the stellar masses we considered. This behavior is the result of the expansion of the radiative zone, allowing the propagation of higher-frequency waves, and the subsequent decrease in stellar density at the convective–radiative interface, which cuts the energy off that is transported by the tidal gravity waves. Then, as the stellar structure stabilizes, tidal dissipation evolves to a stationary value during the MS, which is maximum for K-type stars and decreases by several orders of magnitude for F-type stars because their convective envelope is thinner. We also find that during most of the PMS and the beginning of the MS when the star rotates rapidly, the dissipation of the dynamical tide in the convective zone dominates the other contributions for fast rotators. Then, as magnetic braking spins the star down on the MS, tidal gravity wave dissipation becomes the largest contribution. We confirmed that stellar metallicity also significantly affects tidal dissipation. The dissipation is two orders of magnitude larger in a metal-rich ( $Z = 0.0255$ ) than in a metal-poor star ( $Z = 0.0040$ ). However, we find that at a given age, the dissipation is more efficient in low-metallicity stars during the PMS, SGB, and RGB because they evolve more quickly. Finally, we showed that the contribution of a convective core for F-type stars is negligible compared to the tidal dissipation derived by assuming a bilayer structure. Because tidal dissipation is enhanced by density inhomogeneities in the

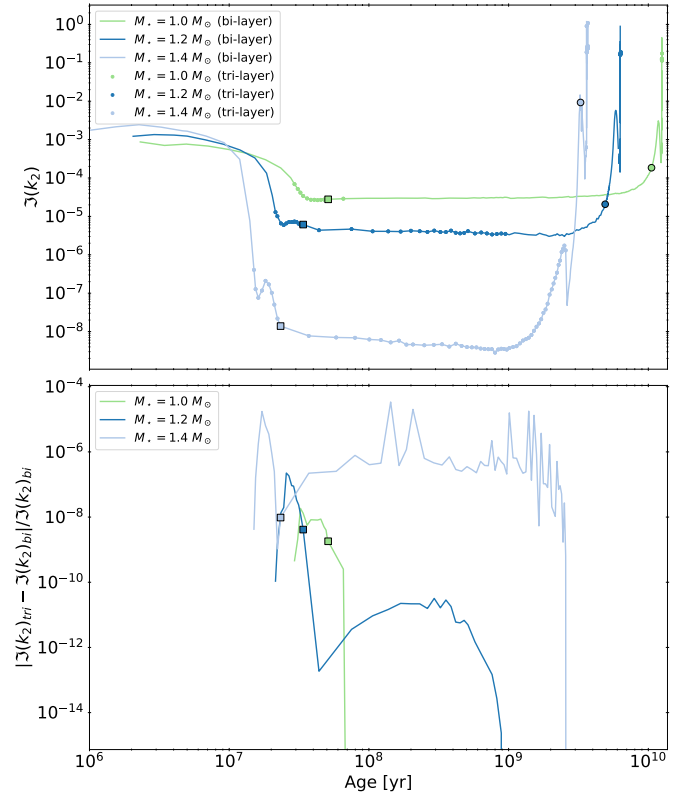


**Fig. 12.** Evolution of tidal dissipation in the case of a bilayer and a trilayer structure. *Top:* evolution of the tidal dissipation in the case of a bilayer (blue curves) and a trilayer (blue dots) structure as a function of time for stellar masses  $M_* = \{1 - 1.4\} M_\odot$ , with  $P_{\text{orb}} = 1$  d. *Bottom:* time evolution of the relative difference of tidal dissipations derived from bilayer and trilayer structures. The colored squares correspond to the ZAMS in each model, and the colored circles show the TAMS.

convective zone (see Eq. (116) for more details), the geometry and mass distribution of a spherically convective core is unfavorable to the excitation and dissipation of tidal gravity waves.

We find that a massive star structure and a solar-type star structure lead to similar prescriptions regarding tidal dissipation. However, this symmetry is made possible by assuming a polytropic behavior of stellar matter at the stellar surface, which leads to a vanishing density there. A more detailed study of the boundary conditions at the surface, detailed in Appendix C, is required to assess the robustness of this analogy.

We also considered a linear approximation of  $N^2$  near the convective–radiative interfaces. Taking more complex  $N^2$  profiles into consideration (Lecoanet & Quataert 2013) may change the frequency dependency of the induced tidal torque and may agree better with 3D numerical simulations of internal wave breaking (Barker 2011; Ivanov et al. 2013). Nonetheless, according to Barker (2011), an improved prescription may deviate from ours by a factor of 2 at most, meaning that our model provides a suitable order of magnitude of the dissipation of tidal gravity waves to follow the secular evolution of a star–planet system.

Taking dissipation processes (Zahn et al. 1997; Barker & Ogilvie 2010) and angular momentum transport in stellar interiors into account (see Mathis & Alvan 2013 for a review) is also one of the perspectives of this work. In this context, we need to factor in stellar rotation (Ogilvie & Lin 2004). Regarding our formulation, adding the Coriolis acceleration may directly

alter the forcing term  $\mathcal{F}$  because gravito-inertial waves are no longer evanescent in a sub-inertial regime (where  $|\omega| < 2\Omega_*$ ) in the convective zone. This effect is expected to increase tidal dissipation in the radiative zone (Rocca 1987, 1989; Ogilvie & Lin 2007; Witte & Savonije 2002). In the same propagation regime, low-frequency waves in the radiative zone are trapped near the equatorial plane, which leads to a geometry that is significantly different from what we considered here (Rieutord & Valdetaro 1997; Dintrans et al. 1999). This change is likely to modify the tidal dissipation accordingly. In addition, because we find that the dissipation through IGW is highest during the radiative core formation when the star is spinning up, a progressive trapping of gravito-inertial waves in the subinertial regime may occur. Stellar rotation also increases the radial wavenumber of the gravito-inertial waves, leading to a stronger radiative damping. These are therefore deposited closer to their excitation region than in the nonrotating case (Pantillon et al. 2007; Mathis et al. 2008).

Differential rotation on tides should also be taken into account because it affects propagation of gravito-inertial waves, leading to a large variety of resonant cavities and chaotic zones (Mathis 2009; Prat et al. 2018). It also allows the deposition of angular momentum in critical layers and therefore interactions between waves and mean flows (Goldreich & Nicholson 1989; Alvan et al. 2013; Astoul et al. 2021). A strong differential rotation may set up during the PMS due to stellar contraction (Charbonnel et al. 2013; Hypolite & Rieutord 2014; Gouhier et al. 2021), when the tidal dissipation through gravity waves is highest. This effect can therefore be significant on the evolution of binary and planetary systems. A magnetic field may also affect tidal dissipation by modifying the propagation and the damping of tidal gravity waves (Mathis & de Brye 2011, 2012).

Despite these limitations, a consistent formulation of the dynamical tide in stellar radiative zones provides a way to an exhaustive study of the fate of star–planet systems. In this spirit, systematically comparing tidal dissipation in radiative and convective zones (Mathis 2015; Gallet et al. 2017) requires a secular evolution model to track the complex evolution of the tidal forcing frequency (Benbakoura et al. 2019). We compared the capacity of the star to dissipate progressive tidal gravity waves in the radiative zone and inertial modes tidally excited in the convective zone. In a more realistic model, we need to estimate the passing of a gravito-inertial wave from one zone to another and possible reflections. This undertaking then requires to take the complex temporal evolution of the tidal frequency into account, which is related to the orbital dynamics of a given system.

In the case of exoplanetary systems, for example, a secular evolution model with a formalism that coherently models tidal effects in stellar convective and radiative zones would allow us to study the migration of nearby planets and their lifetime throughout the stellar evolution, thus reconciling the results of recent studies (e.g., Barker & Ogilvie 2010; Guillot et al. 2014; Barker 2020; Bolmont & Mathis 2016; Gallet et al. 2017; Bolmont et al. 2017; Benbakoura et al. 2019). This approach would ultimately allow us to take other star–planet interactions into account and to explain the observed statistical distributions (McQuillan et al. 2013). The implementation of secular evolution models like this is of primary importance for analyzing data of upcoming space missions such as PLATO (Rauer et al. 2014).

*Acknowledgements.* We would like to thank the referee, Jim Fuller, Allan-Sacha Brun and Antoine Strugarek for helpful comments and suggestions regarding our work. J.A. and S.M. acknowledge the PLATO CNES funding

at CEA/IRFU/DAp. J.A. acknowledges funding from the European Union’s Horizon-2020 research and innovation programme (Grant Agreement no. 776403 Exoplanets-A). S.M. and J.A. acknowledge funding by the European Research Council through the ERC grant SPIRE 647383. L.A. acknowledges funding from the European Research Council AWESoMeStars 682393.

## References

- Abramowitz, M., & Stegun, I. A. 1972, *Handbook of Mathematical Functions* (New York: Dover)
- Alvan, L., Mathis, S., & Decressin, T. 2013, *A&A*, **553**, A86
- Amard, L., Palacios, A., Charbonnel, C., et al. 2016, *A&A*, **587**, A105
- Amard, L., Palacios, A., Charbonnel, C., et al. 2019, *A&A*, **631**, A77
- Asplund, M., Grevesse, N., Sauval, A. J., & Scott, P. 2009, *ARA&A*, **47**, 481
- Astoul, A., Park, J., Mathis, S., et al. 2021, *A&A*, **647**, A144
- Auclair-Desrotour, P., Mathis, S., & Le Poncin-Lafitte, C. 2015, *A&A*, **581**, A118
- Auclair-Desrotour, P., Laskar, J., & Mathis, S. 2017, *A&A*, **603**, A107
- Augustson, K. C., & Mathis, S. 2019, *ApJ*, **874**, 83
- Alvan, L., Strugarek, A., Brun, A. S., Mathis, S., & Garcia, R. A. 2015, *A&A*, **581**, A112
- Barker, A. J. 2011 *MNRAS*, **414**, 1365
- Barker, A. J. 2020 *MNRAS*, **498**, 2
- Barker, A. J., & Ogilvie, G. 2010, *MNRAS*, **404**, 1849
- Beck, P. G., Mathis, S., Gallet, F., et al. 2018, *MNRAS*, **479**, L123
- Benbakoura, M., Réville, V., Brun, A. S., et al. 2019, *A&A*, **621**, A124
- Benomar, O., Takata, M., Shibahashi, H., et al. 2015, *MNRAS*, **452**, 3
- Bolmont, E., & Mathis, S. 2016, *CeMDA*, **126**, 275
- Bolmont, E., Gallet, F., Mathis, S., et al. 2017, *A&A*, **604**, A113
- Brun, A. S., & Zahn, J.-P. 2006, *A&A*, **457**, 665
- Chandrasekhar, S. 1939, *An Introduction of the Study of Stellar Structure* (Chicago: University of Chicago Press)
- Charbonnel, C., Decressin, T., Amard, L., Palacios, A., & Talon, S. 2013, *A&A*, **554**, A40.
- Chernov, S. V., Papaloizou, J. C. B., & Ivanov, P. B. 2013, *MNRAS*, **434**, 1079
- Cowling, T. G. 1941, *MNRAS*, **101**, 367
- Cuntz, M., Saar, S. H., & Musielak, Z. E. 2000, *ApJ*, **533**, L151
- Damiani, C., & Mathis, M. 2018, *A&A*, **618**, A90
- Dintrans, B., Rieutord, M., & Valdetaro, L. 1999, *JFM*, **398**, 271
- Duguid, C. D., Barker, A. J., & Jones, C. A. 2020, *MNRAS*, **497**, 3400
- Essick, R., & Weinberg, N. N. 2016, *ApJ*, **816**, 18
- Fröman, F., & Fröman, P. O. 1965, *JWKB Approximation: Contributions to the Theory* (Amsterdam: North-Holland)
- Fuller, J. 2017, *MNRAS*, **472**, 1538
- Fuller, J., Lecoanet, D., Cantiello, M., & Brown, B. 2014, *ApJ*, **796**, 17
- Gallet, F., & Bouvier, J. 2015, *A&A*, **577**, A98
- Gallet, F., Bolmont, E., Mathis, S., Charbonnel, C., & Amard, L. 2017, *A&A*, **604**, A112
- Goldreich, P. 1963, *MNRAS*, **126**, 257
- Goldreich, P., & Nicholson, P. D. 1989, *ApJ*, **342**, 1079
- Gonzalez, G. 1997, *MNRAS*, **285**, 403
- Goodman, J., & Dickson, E. S. 1998, *ApJ*, **507**, 938
- Gouhier, B., Lignières, F., & Jouve, L. 2021, *A&A*, **648**, A109
- Guillot, T., Lin, D. N. C., Morel, P., et al. 2014, in *EAS Pub. Ser.*, **65**, 327
- Hypolite, D., & Rieutord, M. 2014, *A&A*, **572**, A15
- Ivanov, P. B., Papaloizou, J. C. B., & Chernov, S. V. 2013, *MNRAS*, **432**, 3, 2339
- Kaula, W. M. 1964, *Rev. Geophys.*, **2**, 661
- Kawaler, S. D. 1988, *ApJ*, **333**, 236
- Kippenhahn, R., & Weigert, A. 1994, *Stellar Structure and Evolution* (Berlin: Springer)
- Kushnir, D., Zaldarriaga, M., Kollmeier, J. A., & Waldman, R. 2017, *MNRAS*, **467**, 2146
- Lagarde, N., Decressin, T., Charbonnel, C., et al. 2012, *A&A*, **543**, A108
- Lai, D. 2012, *MNRAS*, **423**, 486
- Lebreton, Y., Goupil, M. J., & Montalbán, J., 2014, in *EAS Pub. Ser.*, **65**, The *Ages of Stars*, eds. Y. Lebreton, D. Valls-Gabaud, & C. Charbonnel
- Lecoanet, D., & E. Quataert, E. 2013, *MNRAS*, **430**, 2363
- Lecoute, J., Chabrier, G., Baraffe, I., & Levrard, B. 2010, *A&A*, **516**, A64
- MacDonald, G. J. F. 1964, *Rev. Geophys.*, **2**, 467
- Mathis, S. 2009, *A&A*, **506**, 811
- Mathis, S. 2015, *A&A*, **580**, L3
- Mathis, S. 2019, in *EAS Pub. Ser.*, **82**, *Astro Fluid: An International Conference in Memory of Professor Jean-Paul Zahn’s Great Scientific Achievements*, eds. A. S. Brun, S. Mathis, C. Charbonnel, & B. Durrille
- Mathis, S., & Alvan, L. 2013, in *ASP Conf. Ser.*, **479**, *Progress in Physics of the Sun and Stars: A New Era in Helio- and Asteroseismology*, 295, eds. H. Shibahashi, & A. E. Lynas-Gray
- Mathis, S., & de Brye, N. 2011, *A&A*, **526**, A65

- Mathis, S., & de Brye, N. 2012, [A&A](#), **540**, [A37](#)
- Mathis, S., Talon, S., Pantillon, F. P., et al. 2008 [J. Phys. Conf. Ser.](#), **118**, [1](#)
- Mathis, S., Auclair-Desrotour, P., Guenel, M., Gallet, F., & Le Poncin-Lafitte, C. 2016, [A&A](#), **592**, [A33](#)
- Matt, S. P., Brun, A.-S., Baraffe, I., Bouvier, J., & Chabrier, G. 2015, [ApJ](#), **799**, [L23](#)
- McQuillan, A., Mazeh, T., & Aigrain, S., 2013, [ApJ](#), **775**, [L11](#)
- Morel, P., & Lebreton, Y. 2008, [Ap&SS](#), **316**, [61](#)
- Murray, C. D., & Dermott, S. F. 1999, [Solar System Dynamics](#) (Cambridge University Press)
- North, P., & Zahn, J.-P., 2003, [A&A](#), **405**, [677](#)
- Ogilvie, G. I. 2013, [MNRAS](#), **429**, [613](#)
- Ogilvie, G. I. 2014, [ARAA](#), **52**, [171](#)
- Ogilvie, G. I., & Lin, D. N. C., 2004, [ApJ](#), **610**, [477](#)
- Ogilvie, G. I., & Lin, D. N. C. 2007, [MNRAS](#), **661**, [1180](#)
- Pantillon, F. P., Talon, S., & Charbonnel, C. 2007, [A&A](#), **474**, [155](#)
- Papaloizou, J. C. B., & Savonije, G. J. 1985, [MNRAS](#), **213**, [85](#)
- Papaloizou, J. C. B., & Savonije, G. J. 1997, [MNRAS](#), **291**, [651](#)
- Prat, V., Mathis, S., Augustson, K., et al. 2018, [A&A](#), **615**, [A106](#)
- Press, W. H. 1981, [ApJ](#), **245**, [286](#)
- Rauer, H., Catala, C., Aerts, C., et al. 2014, [Exp. Astron.](#), **38**, [249](#)
- Remus, F., Mathis, S., & Zahn, J.-P. 2012, [A&A](#), **544**, [132](#)
- Rieutord, M., & Valdetarro, L. 1997, [JFM](#), **341**, [01](#)
- Rocca, A., 1987, [A&A](#), **175**, [81](#)
- Rocca, A., 1989, [A&A](#), **213**, [114](#)
- Rogers, T. M., Lin, D. N. C., McElwaine, J. N., & Lau, H. H. B. 2013, [ApJ](#), **772**, [21](#)
- Sadeghi Ardestani, L., Guillot, T., & Morel, P. 2017, [MNRAS](#), **472**, [2590](#)
- Santos, N. C., Israelian, G., Mayor, M., Rebolo, R., & Udry, S. 2003, [A&A](#), **398**, [363](#)
- Savonije, G. J., & Papaloizou, J. C. B. 1983, [MNRAS](#), **203**, [581](#)
- Savonije, G. J., & Papaloizou, J. C. B. 1984, [MNRAS](#), **207**, [685](#)
- Savonije, G. J., & Papaloizou, J. C. B. 1997, [MNRAS](#), **291**, [633](#)
- Savonije, G. J., Papaloizou, J. C. B., & Alberts, F. 1995, [MNRAS](#), **277**, [471](#)
- Schlaufman, K. C., & Winn, J. N., 2013, [ApJ](#), **772**, [143](#)
- Schneider, J., Dedieu, C., Le Sidaner, P., Savalle, R., & Zolotukhin, I. 2011, [A&A](#), **532**, [A79](#)
- Skumanich, A. 1972, [ApJ](#), **171**, [565](#)
- Siess, L., Dufour, E., & Forestini, M. 2000, [A&A](#), **358**, [593](#)
- Spiegel, E. A., & Veronis, G. 1960, [ApJ](#), **131**, [442](#)
- Stevenson, D. J. 1979, [GApFD](#), **12**, [139](#)
- Strugarek, A., Brun, A. S., Matt, S. P., & Réville, V., 2014, [ApJ](#), **795**, [86](#)
- Strugarek, A., Brun, A. S., Matt, S. P., & Réville, V. 2015, [ApJ](#), **815**, [111](#)
- Strugarek, A., Bolmont, E., Mathis, S., et al. 2017, [ApJ](#), **847**, [2](#)
- Terquem C., Papaloizou, J. C. B., Nelson, R. P., & Lin, D. N. C. 1998, [ApJ](#), **502**, [788](#)
- Valdetarro, L., Rieutord, M., Braconnier, T., & Fraysse, V. 2007, [J. Comput. Appl. Math.](#), **205**, [382](#)
- Vick, M., & Lai, D. 2020, [MNRAS](#), **496**, [3](#)
- Weinberg, N. N., Sun, M., Arras, P., & Essick, R. 2017, [ApJ](#), **849**, [L11](#)
- Witte, M.G., & Savonije, G. J. 2002, [A&A](#), **386**, [222](#)
- Zahn, J. P. 1970, [A&A](#), **29**, [489](#)
- Zahn, J. P. 1975, [A&A](#), **4**, [452](#)
- Zahn, J. P. 1975, [A&A](#), **41**, [329](#)
- Zahn, J.-P. 1977, [A&A](#), **57**, [383](#)
- Zahn, J.-P., Talon, S., & Matias, J. 1997, [A&A](#), **322**, [320](#)

## Appendix A: Computation of a particular solution in the radiative zone near the interface

The goal of this section is to compute a particular solution of Eq. (20) in the radiative zone, near the interface. In this configuration, Eq. (20) becomes

$$\frac{d^2\psi}{d\eta^2} + v^2\eta\psi = v^2\eta Z. \quad (\text{A.1})$$

For a given function  $f$ , we write in this section  $\frac{df}{d\eta} = f'$ . We choose  $\psi_1(\eta) = \text{Ai}[v^{\frac{2}{3}}(-\eta)]$  and  $\psi_2(\eta) = \text{Bi}[v^{\frac{2}{3}}(-\eta)]$  as the two basis solutions of the corresponding homogeneous equation. Their Wronskian  $\Lambda_A$  can be written as

$$\Lambda_A = \psi_1\psi_2' - \psi_2\psi_1' = -\frac{v^{\frac{2}{3}}}{\pi}. \quad (\text{A.2})$$

Then a particular solution of the inhomogeneous Airy equation that vanishes at the interface can be expressed as

$$\begin{aligned} \psi_p(\eta) = & - \left( \int_0^\eta \Lambda_A^{-1} v^2 \eta Z \psi_2(\eta) d\eta \right) \psi_1(\eta) \\ & + \left( \int_0^\eta \Lambda_A^{-1} v^2 \eta Z \psi_1(\eta) d\eta \right) \psi_2(\eta). \end{aligned} \quad (\text{A.3})$$

From Eq. (A.1) we obtain

$$\frac{\psi_p(\eta)}{v^{-\frac{2}{3}}\pi} = \left( \int_0^\eta -Z\psi_2''(\eta) d\eta \right) \psi_1(\eta) + \left( \int_0^\eta Z\psi_1''(\eta) d\eta \right) \psi_2(\eta), \quad (\text{A.4})$$

which leads to

$$\begin{aligned} \frac{\psi_p(\eta)}{v^{-\frac{2}{3}}\pi} = & -Z(\eta)\Lambda_A + Z(0) [\psi_2'(0)\psi_1(\eta) - \psi_1'(0)\psi_2(\eta)] \\ & + [Z'\psi_2]_0^\eta \psi_1 - [Z'\psi_1]_0^\eta \psi_2 + \mathcal{I}, \end{aligned} \quad (\text{A.5})$$

with  $\mathcal{I} = -\left(\int_0^\eta Z''\psi_2(\eta) d\eta\right)\psi_1 + \left(\int_0^\eta Z''\psi_1(\eta) d\eta\right)\psi_2$ . This term is neglected from now on by assuming that the equilibrium tide varies slower than the dynamical tide in the radiative zone. Because  $\psi_1'(0) = -v^{\frac{2}{3}}\text{Ai}'(0)$  and  $\psi_2'(0) = -v^{\frac{2}{3}}\text{Bi}'(0)$ , we obtain

$$\begin{aligned} \psi_p(\eta) = & Z(\eta) - Z(0)\pi [\text{Bi}'(0)\psi_1(\eta) - \text{Ai}'(0)\psi_2(\eta)] \\ & - v^{-\frac{2}{3}}\pi Z'(0) [\text{Bi}(0)\psi_1(\eta) - \text{Ai}(0)\psi_2(\eta)]. \end{aligned} \quad (\text{A.6})$$

We know that  $\pi = [\text{Ai}(0)\text{Bi}'(0) - \text{Bi}(0)\text{Ai}'(0)]^{-1} = \frac{1}{2}3^{\frac{3}{2}}\Gamma\left(\frac{4}{3}\right)\Gamma\left(\frac{2}{3}\right)$ , therefore the particular solution becomes

$$\psi_p(\eta) = Z(\eta) + \left(\frac{\tau}{2}\right)^{\frac{1}{3}} \left[ \alpha_{\text{rad,p}} J_{\frac{1}{3}}(\tau) + \beta_{\text{rad,p}} J_{-\frac{1}{3}}(\tau) \right], \quad (\text{A.7})$$

where  $\alpha_{\text{rad,p}} = -\frac{dZ}{d\eta}(0) \left(\frac{v}{3}\right)^{-\frac{2}{3}} \Gamma\left(\frac{4}{3}\right)$  and  $\beta_{\text{rad,p}} = -Z(0)\Gamma\left(\frac{2}{3}\right)$ .

## Appendix B: Forcing term and radial displacement for a low-mass star

We aim in this section to link the forcing term to the radial displacement that is connected to the dynamical tide. This compares formulations from Zahn (1975) and Goodman & Dickson (1998). The derivative of the radial displacement at the interface linked to the dynamical tide can be expressed with the notations we used in Sect. 2,

$$\partial_r \xi_r^{\text{dyn}} \Big|_{\text{int}} = \partial_r \left[ \rho_0^{-\frac{1}{2}} r^{-2} (\rho_0^{-\frac{1}{2}} X - Z) \right]_{\text{int}}. \quad (\text{B.1})$$

By expressing the radial displacement  $\xi_r$  in the  $(S_+, S_-)$  basis, knowing that  $\mathcal{T}_1 = 0$ , we obtain from Eqs. (44), (60) and (63)

$$\begin{aligned} \partial_r \xi_r^{\text{dyn}} \Big|_{\text{int}} = & \partial_r \left( \rho_0^{-\frac{1}{2}} r^{-2} \right) \Big|_{\text{int}} \left[ \frac{\beta_{\text{conv}} + \beta_{\text{conv,p}}}{\Gamma\left(\frac{2}{3}\right)} - Z(0) \right] \\ & + \rho_0^{-\frac{1}{2}} (r_{\text{int}}) r_{\text{int}}^{-2} \left[ \frac{\beta_{\text{conv}} + \beta_{\text{conv,p}}}{\Gamma\left(\frac{2}{3}\right)} \frac{d}{dr} (\rho_0^{-\frac{1}{2}} X_h)_{\text{int}} + \mathcal{T} - \partial_r Z(0) \right] \end{aligned} \quad (\text{B.2})$$

with

$$\begin{aligned} \mathcal{T} = & \rho_0^{\frac{1}{2}} (r_{\text{int}}) r_{\text{int}}^2 \left\{ -\frac{\rho_0'(r_{\text{int}})}{\rho_0(r_{\text{int}})} - \frac{(\rho_0^{-\frac{1}{2}} Z)_{\text{int}}'}{(\rho_0^{-\frac{1}{2}} Z)_{\text{int}}} + \frac{X_1'(r_{\text{int}})}{X_1(r_{\text{int}})} \right\} \left( \frac{\varphi_T}{g} \right)_{\text{int}} \\ & + \rho_0^{\frac{1}{2}} (r_{\text{int}}) \mathcal{F}. \end{aligned} \quad (\text{B.3})$$

Because  $C_2 = 0$ , the homogeneous solution  $X_h$  in the convective zone is proportional to the basis solution  $X_1$ , which leads to

$$\partial_r \xi_r^{\text{dyn}} = \frac{\partial_r (\rho_0^{-1} r^{-2} X_h) \Big|_{\text{int}}}{\rho_0^{-1} r^{-2} X_h \Big|_{\text{int}}} \xi_r^{\text{dyn}}(r_{\text{int}}) + r_{\text{int}}^{-2} \mathcal{F}, \quad (\text{B.4})$$

where  $\xi_r^{\text{dyn}}(r_{\text{int}}) = \rho_0^{-\frac{1}{2}} (r_{\text{int}}) r_{\text{int}}^{-2} \left( \frac{\beta_{\text{conv}} + \beta_{\text{conv,p}}}{\Gamma\left(\frac{2}{3}\right)} - Z(0) \right)$ . By

assuming slow variations of the density and the radius compared to the characteristic length of variation of the gravity waves in the radial direction  $\lambda = v^{-\frac{2}{3}} = \omega^{\frac{2}{3}} [l(l+1)]^{-\frac{1}{3}} \left| \frac{dN^2}{d \ln r} \right|_{r_{\text{int}}}^{-\frac{1}{3}} r_{\text{int}}$  (Goodman & Dickson 1998; Kushnir et al. 2017), we obtain from Eq. (44)

$$\partial_r \xi_r^{\text{dyn}} \Big|_{\text{int}} \sim \frac{\Gamma\left(\frac{2}{3}\right)}{3^{\frac{2}{3}} \Gamma\left(\frac{4}{3}\right) \beta_{\text{conv}}} \frac{\alpha_{\text{conv}} \xi_r^{\text{dyn}}(r_{\text{int}})}{\lambda} + r_{\text{int}}^{-2} \mathcal{F}. \quad (\text{B.5})$$

Because  $\xi_r^{\text{dyn}}(r_{\text{int}}) \sim \lambda \partial_r \xi_r^{\text{dyn}} \Big|_{\text{int}}$  (Goodman & Dickson 1998) and  $\alpha_{\text{conv}} \ll \beta_{\text{conv}}$ , we have

$$\partial_r \xi_r^{\text{dyn}} \Big|_{\text{int}} \sim r_{\text{int}}^{-2} \mathcal{F}, \quad (\text{B.6})$$

which ensures the equivalence between the formulations from Zahn (1975) and Goodman & Dickson (1998).

### Appendix C: Stress-free condition at the stellar surface

The goal of this section is to investigate the consequences on tidal dissipation of low-mass stars of a stress-free boundary condition coupled with a nonzero density at the stellar surface. In this case, the Lagrangian perturbation of pressure vanishes at  $r = R_\star$ ,

$$\delta P = \rho_0(R_\star) [y - g_0(R_\star)\xi_r(R_\star)] = 0. \quad (\text{C.1})$$

We considered the case where  $\rho_0(R_\star) > 0$  and  $\frac{\rho'_0(R_\star)}{\rho_0(R_\star)}$  is the only large parameter involved to account for the density behavior near the photosphere. From Eqs. (12) in the anelastic approximation, we obtain

$$\xi_r(R_\star) = -\frac{\varphi_T(R_\star)}{g_0(R_\star)} + \frac{\omega^2}{\omega_{\text{dyn}}^2} \frac{1}{l(l+1)R_\star} \partial_r(r^2 \xi_r). \quad (\text{C.2})$$

By assuming low-frequency waves, *i.e.*  $\omega \ll \omega_{\text{dyn}}$ , the stress-free condition becomes

$$X(R_\star) = -\rho_0(R_\star) R_\star^2 \frac{\varphi_T(R_\star)}{g_0(R_\star)}, \quad (\text{C.3})$$

which accounts for the equilibrium tide. In the convective zone, we choose the basis solution  $X_1$  as the solution of the homogeneous equation associated with Eq. (35) verifying  $X_1(R_\star) = X(R_\star)$  and  $X'_1(R_\star) = X'(R_\star)$ . In this way, we fix  $C_2 = \mathcal{T}_0 = \mathcal{T}_2 = 0$ . As in Sect. 5.1, near the surface,  $X_1$  is a solution of the following equation:

$$X'' - \frac{\rho'_0}{\rho_0} X' = 0, \quad (\text{C.4})$$

which leads to  $X'_1 \propto \rho_0$ . We now impose that  $X'(R_\star) = X'_1(R_\star) = R_\star^2 \rho_0(R_\star)$ . When we assume that the interface between convective and radiative zone is close to the stellar surface, we can assume that

$$\begin{aligned} X'_1(r) &= R_\star^2 [\rho_0(R_\star) + \rho'_0(R_\star)(r - R_\star)] \\ X_1(r) &= X_1(R_\star) + R_\star^2 \left[ \rho_0(R_\star)(r - R_\star) + \frac{1}{2} \rho'_0(R_\star)(r - R_\star)^2 \right]. \end{aligned} \quad (\text{C.5})$$

These expressions are adopted as a boundary condition in our numerical treatment of tidal dissipation to consider the surface singularity in the case of solar-type stars. Furthermore, when we assume that  $\frac{\rho_0(R_\star)}{\rho'_0(R_\star)} \ll R_\star^2 (\alpha - 1)^2$ , we obtain

$$\frac{X'_1(R_\star)}{X_1(r_{\text{int}})} = \frac{1}{-\frac{\varphi_T(R_\star)}{g(R_\star)} + R_\star(\alpha - 1) + \frac{1}{2} \frac{\rho'_0(R_\star)}{\rho_0(R_\star)} R_\star^2 (\alpha - 1)^2} \ll 1, \quad (\text{C.6})$$

$$\frac{X_1(R_\star)}{X_1(r_{\text{int}})} = \frac{-\frac{\varphi_T(R_\star)}{g(R_\star)}}{-\frac{\varphi_T(R_\star)}{g(R_\star)} + R_\star(\alpha - 1) + \frac{1}{2} \frac{\rho'_0(R_\star)}{\rho_0(R_\star)} R_\star^2 (\alpha - 1)^2} \ll 1. \quad (\text{C.7})$$

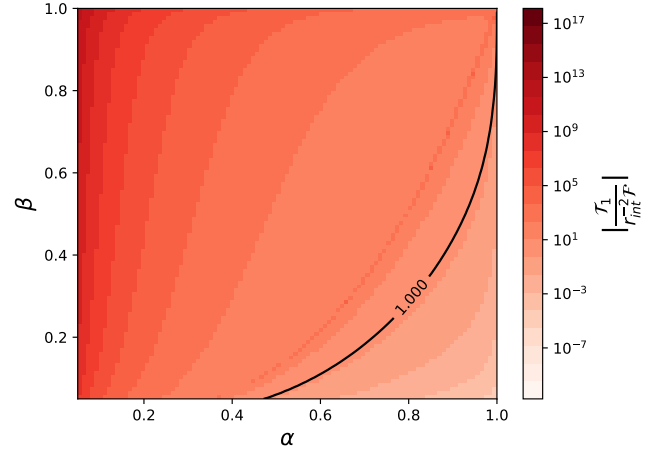


**Fig. C.1.** Value of  $\mathcal{T}_1/r_{\text{int}}^{-2}\mathcal{F}$  for all the possible values of  $\alpha = R_r/R_\star$  and  $\beta = M_r/M_\star$ . In black we show values of  $\alpha$  and  $\beta$  for which the ratio is equal to 1.

The  $\mathcal{T}_1$  term then becomes

$$\begin{aligned} \mathcal{T}_1 &= \frac{\varphi_T(R_\star)}{g(R_\star)} \alpha^{-2} \frac{\rho'_0(R_\star)}{\rho_0(R_\star)} \frac{X_1(R_\star)}{X_1(r_{\text{int}})} \\ &\sim -2 \left( \frac{\varphi_T(R_\star)}{g(R_\star)} \right)^2 \alpha^{-2} (1 - \alpha)^{-2} R_\star^{-2}. \end{aligned} \quad (\text{C.8})$$

Furthermore, in the case of a thin convective layer, we have from Eq. (127)

$$r_{\text{int}}^{-2}\mathcal{F} = 3 \frac{1 - \gamma}{1 - \alpha} \alpha^5 \left( \frac{2\alpha}{3} - 1 \right) \alpha^{-2} \frac{\varphi_T(R_\star)}{g(R_\star)} R_\star^{-1}. \quad (\text{C.9})$$

Then we obtain

$$\frac{\mathcal{T}_1}{r_{\text{int}}^{-2}\mathcal{F}} = -\frac{2}{3} \frac{\beta}{\alpha^5 (1 - \gamma)(1 - \alpha)} \left( \frac{2\alpha}{3} - 1 \right) \frac{\varphi_T(R_\star)}{g(R_\star)} R_\star^{-1}. \quad (\text{C.10})$$

Because  $\gamma = \frac{\alpha^3(1-\beta)}{\beta(1-\alpha^3)}$ , we have

$$\frac{\mathcal{T}_1}{r_{\text{int}}^{-2}\mathcal{F}} = -\frac{2}{3} \frac{\beta^2(1 + \alpha + \alpha^2)}{\alpha^5 \left( \frac{2\alpha}{3} - 1 \right) (\beta - \alpha^3)} \frac{\varphi_T(R_\star)}{g(R_\star)} R_\star^{-1}. \quad (\text{C.11})$$

The values of this ratio for all the possible values of  $\alpha = R_r/R_\star$  and  $\beta = M_r/M_\star$  are represented in Fig. C.1. As we assumed that the convective zone is sufficiently thin to linearize the density profile, only values of  $\alpha$  close to 1 are relevant in this analysis. Therefore we can assume that the  $\mathcal{T}_1$  term affects our prescription for tidal dissipation only marginally in the radiative zone in the case of a surface density that is sufficiently weak. A more detailed study of surface boundary conditions is left for future work.

## Appendix D: Wave-breaking criterion for solar-type stars

To provide a general criterion for wave braking in the case of solar-type stars, we rely on the nonlinearity factor  $\epsilon_{nl}$ , which is the ratio of the amplitude of the radial displacement to the radial wavelength (Press 1981; Barker & Ogilvie 2010; Barker 2020),

$$\epsilon_{nl} = |k_r \xi_r|. \quad (\text{D.1})$$

Nonlinearities become significant when  $\epsilon_{nl} \geq 1$ . In particular, wave braking is likely to occur. This nonlinearity factor can be assessed through the energy luminosity of the tidal gravity wave. We have from Eq. (75)

$$|L_E| = \frac{\omega^3}{2l(l+1)} |C_W|^2. \quad (\text{D.2})$$

Furthermore, by defining  $\xi_r^{\text{dyn}}$  the radial displacement linked to the dynamical tide, we obtain in the WKB approximation

$$\xi_r^{\text{dyn}}(r) = \rho_0^{-\frac{1}{2}} r^{-2} C_W \frac{1}{\sqrt{k_r}} e^{\epsilon i(\tau_w - \tau_0)}, \quad (\text{D.3})$$

where  $k_r \approx \sqrt{\frac{N^2}{\omega^2} \frac{l(l+1)}{r^2}}$  is the radial wavenumber. This leads to

$$|C_W|^2 = \rho_0 r^3 \frac{N}{\omega} \sqrt{l(l+1)} \left| \xi_r^{\text{dyn}} \right|^2. \quad (\text{D.4})$$

The energy luminosity then becomes

$$|L_E| = \frac{N \omega^2 \rho_0 r^3}{2 \sqrt{l(l+1)}} \left| \xi_r^{\text{dyn}} \right|^2. \quad (\text{D.5})$$

We can therefore assess  $\epsilon_{nl}$  as

$$\epsilon_{nl} = \sqrt{\frac{2[l(l+1)]^{\frac{3}{2}} N |L_E|}{\rho_0 r^5 \omega^4}}, \quad (\text{D.6})$$

which is similar to the expression obtained in Eq. (53) in Barker (2020). Furthermore, in the case of a solar-type star, we find that the energy luminosity  $L_E$  is equal to

$$L_E = -\frac{3^{\frac{2}{3}} \Gamma^2 \left( \frac{1}{3} \right)}{8\pi} \omega^{\frac{11}{3}} [l(l+1)]^{-\frac{4}{3}} \rho_0(r_{\text{int}}) r_{\text{int}} \left| \frac{dN^2}{d \ln r} \right|_{r_{\text{int}}}^{-\frac{1}{3}} \mathcal{F}^2, \quad (\text{D.7})$$

with

$$\mathcal{F} = \int_{r_{\text{int}}}^{R_*} \left[ \left( \frac{r^2 \varphi_T}{g_0} \right)'' - \frac{l(l+1)}{r^2} \left( \frac{r^2 \varphi_T}{g_0} \right) \right] \frac{X_1}{X_1(r_{\text{int}})} dr. \quad (\text{D.8})$$

As  $L_E \propto \mathcal{F}^2$ , we introduce  $|L_E| = L_{E,0} m_p^2 n^4 \omega^{\frac{11}{3}}$ , where  $L_{E,0}$  is independent of the tidal frequency and planetary properties,  $m_p$  is the planetary mass, and  $n$  the mean motion of its orbit. This means that wave braking may occur if  $\epsilon_{nl} \geq 1$ , which leads to

$$\frac{2[l(l+1)]^{\frac{3}{2}} N L_{E,0} m_p^2 n^4}{\rho_0 r^5} \omega^{-\frac{1}{3}} \geq 1. \quad (\text{D.9})$$

In the absence of stellar rotation, we have  $\omega = 2n$ . Furthermore, near the stellar center, the radial profile of the Brunt–Väisälä is approximately linear. We then assume that  $N \approx Cr$ , where

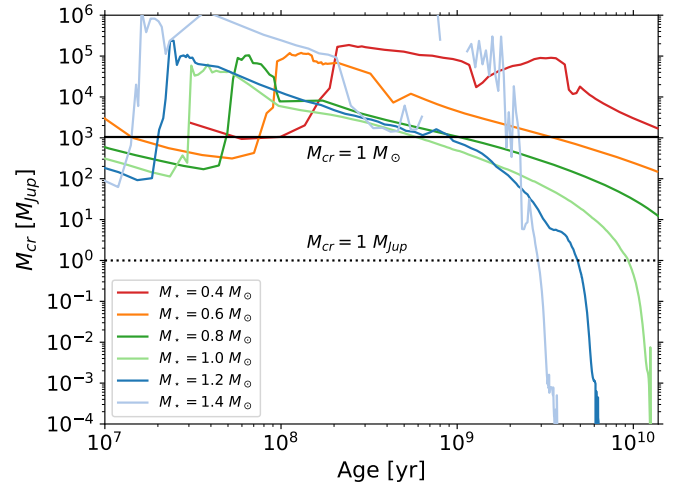


**Fig. D.1.** Evolution of the critical planetary mass  $M_{cr}$  as a function of the age of the system for stellar masses ( $M_*$ ) between 0.4 and  $1.4 M_\odot$ . Wave braking may occur for planetary masses higher than  $M_{cr}$ .

$C \approx 8 \times 10^{-11} \text{ m}^{-1} \text{ s}^{-1}$  for the current Sun (Barker 2020). This quantity is here estimated at a given stellar mass and stellar age by relying on STAREVOL grids. Following Goodman & Dickson (1998), we can estimate the location  $r_{\text{inner}}$  of the inner turning point, defined as  $N = \omega$ , as follows:

$$r_{\text{inner}} = \frac{2n}{C}. \quad (\text{D.10})$$

Then, estimating the nonlinearity factor at the inner turning point gives

$$\frac{2^{-\frac{10}{3}} [l(l+1)]^{\frac{3}{2}} C^5 L_{E,0} m_p^2 n^{-\frac{1}{3}}}{\rho_0(r_{\text{inner}})} \geq 1 \quad (\text{D.11})$$

which, by introducing the orbital period  $P_{\text{orb}}$ , gives the following criterion on the planetary mass:

$$m_p \geq (2\pi)^{\frac{1}{6}} \frac{2^{\frac{5}{3}} \rho_0(r_{\text{inner}})}{[l(l+1)]^{\frac{3}{2}} C^{\frac{5}{2}} L_{E,0}^{\frac{1}{2}}} P_{\text{orb}}^{-\frac{1}{6}} \equiv M_{cr}. \quad (\text{D.12})$$

We then find a similar result as the Barker & Ogilvie (2010) criterion (see also Barker 2011, 2020), which is based on an overturning of the stratification. This condition weakly depends on the orbital period (a decrease by one order of magnitude in  $P_{\text{orb}}$  leads to an increase of  $M_{cr}$  of about 31.9%). If a given planet has a mass higher than  $M_{cr}$ , then wave braking may occur in the star, and the tidal quality factor is expected to behave according to the results of our work. Otherwise, other dissipation processes such as radiative damping in the case of progressive waves or critical layers may lead to a similar tidal dissipation. We present in Fig. D.1 the evolution of  $M_{cr}$  as a function of the age of the system for stellar masses ( $M_*$ ) between 0.4 and  $1.4 M_\odot$ . As was pointed out in Barker (2020), for stellar masses higher than  $0.9 M_\odot$ , the critical planetary mass may fall below 1 Jupiter mass for all ages greater than 10 Gyr. It then allows super-Earths and hot Neptunes to trigger wave braking in their host stars during the subgiant phase and the RGB.

## Appendix E: Angular momentum transport and tidal torque

The goal of this section is to clarify the relationship between the angular momentum transport and the net torque applied to the radiative zone. To this end, we considered a radiative zone between  $r = r_0$  and  $r = r_1 > r_0$ . The equation for the transport of angular momentum, horizontally averaged and focusing only on waves, is given by Mathis (2009),

$$\rho_0 \frac{d}{dt} \left( r^2 \int_{\theta=0}^{\theta=\pi} \sin^3 \theta \Omega d\theta \right) = -\frac{1}{2\pi r^2} \partial_r \left( r^2 \int_{\theta=0}^{\theta=\pi} F_J \sin \theta d\theta \right), \quad (\text{E.1})$$

where  $\Omega$  is the angular velocity of the radiative zone and  $F_J$  is the radial component of flux of angular momentum transported by the Reynolds stresses of the gravity waves, whose expression is given in Eq. (78). By integrating along the radial and latitudinal directions, this leads to

$$\frac{dJ_{\text{RZ}}}{dt} = - \int_{r_0}^{r_1} (\partial_r L_J) dr, \quad (\text{E.2})$$

where  $J_{\text{RZ}} = \rho_0 \int_{r=r_0}^{r=r_1} \int_{\theta=0}^{\theta=\pi} \int_{\varphi=0}^{\varphi=2\pi} r^4 \sin^3 \theta \Omega d\varphi d\theta dr$  is the total angular momentum of the radiative zone and  $L_J = 2\pi \int_{\theta=0}^{\theta=\pi} r^2 F_J \sin \theta d\theta$  is the luminosity of angular momentum.

Hence we obtain

$$\frac{dJ_{\text{RZ}}}{dt} = L_J(r_0) - L_J(r_1). \quad (\text{E.3})$$

In the case of an inward energy transport ( $\epsilon = 1$ , corresponding to the configuration of solar-type stars), tidal gravity waves are excited at  $r = r_1$  and are totally dissipated before reaching the radius  $r = r_0$ . Hence we obtain

$$\frac{dJ_{\text{RZ}}}{dt} = -L_J(r_1). \quad (\text{E.4})$$

In the case of an outward energy transport ( $\epsilon = -1$ , corresponding to the massive and intermediate-mass stars' configuration), tidal gravity waves are excited at  $r = r_0$  and are totally dissipated before reaching the radius  $r = r_1$ . In this configuration, we have

$$\frac{dJ_{\text{RZ}}}{dt} = L_J(r_0). \quad (\text{E.5})$$

This means that we can compute the torque  $T$  applied to the whole radiative zone with a single expression,

$$T = -\epsilon L_{J,\text{exc}}, \quad (\text{E.6})$$

where  $L_{J,\text{exc}}$  is the luminosity of angular momentum estimated in the excitation region of tidal gravity waves.